Front. Earth Sci. 2024, 18(3): 488–508
https://doi.org/10.1007/s11707-022-1054-6

RESEARCH ARTICLE

Controls on the facies and architecture evolution of a fan delta in Qinghai Lake, China

Di MA[1], Xinghe YU[1], Shunli LI (✉)[1], Zhijie ZHANG[2], Chao FU[1], Hongwei SUN[1], Chun LIU[2]

1 School of Energy, China University of Geosciences, Beijing 100083, China
2 Research Institute of Petroleum Exploration and Development, Hangzhou 310000, China

Abstract Deltaic sedimentary systems form the most favorable hydrocarbon reservoirs in continental faulted lacustrine basins, and their types and controlling factors directly affect the distribution of hydrocarbons. The systematic study of typical modern delta deposition provides significant guidance regarding the distribution of oil and gas reservoirs in the subsurface. For this reason, the Heima River delta in Qinghai Lake, which features multiple sediment sources and clear sedimentary evolution stages, was selected for this research. A detailed study of the sedimentology and architectural characteristics of the Heimahe delta in Qinghai Lake was conducted. A total of 4 types of gravel facies, 4 types of sand facies, and 2 types of mud facies were identified. This study also focuses on recognizing the architectural elements within channels and bars. The delta plain features debris-flow, switched, and migrated channels and vertical and bilateral aggradation bars. The delta front features migrated and filled channels and bilateral and lateral aggradation bars. Twenty-two representative outcrop sections were selected. Detailed observation and analysis of these sections revealed three stages: the progradation to aggradation (PA) stage, in which the deposits show evidence of sigmoid-type and coarse-grained sedimentation; the retrogradation (R) stage, which is characterized by imbricated regression; and the aggradation to progradation and degradation (APD) stage, which is characterized by a terraced-stepping, progression stacking pattern. Based on the integrated analysis of the sedimentary environment, outcrop lithofacies associations, architecture stacking patterns, fossils and bioclasts, we identified diverse depositional associations and constructed a sedimentary evolution model of the depositional system in this area. We suggest that the depositional system transitioned from an early single-provenance gravel-rich fan delta to a multi-provenance mud-rich delta and that two factors mainly controlled the transition: the southern boundary fault activity and lake level variations. The contemporaneous activity of the fault increased the accommodation in the low-stand systems tract, which resulted in continuous coarse-sediment deposition.

Keywords Qinghai Lake, Heimahe Delta, sedimentary pattern, controlling factor, Quaternary

1 Introduction

In recent years, discussion of the mechanisms, sedimentary characteristics, architectural characteristics, and controlling factors of deltas has been continuous (Nocita and Lowe, 1990; Horton and Schmitt, 1996; García-García et al., 2006; Winsemann et al., 2007; Rohais et al., 2008; Backert et al., 2010; Eilertsen et al., 2011; García-García et al., 2011; Tan et al., 2016; Yu et al., 2018b). In the study of sedimentary systems, outcrops have the unique advantage of being visual, specific, and indicative of the overall situation (Rioult et al., 1991; Bridge et al., 2000; Miall, 2002; Nagendra et al., 2002; Young et al., 2003; Homewood et al., 2008; Fabuel-Perez et al., 2009; Bemis et al., 2014; Tan et al., 2016; Burnham and Hodgetts, 2019; Freitas et al., 2021). Describing the sedimentary characteristics of typical outcrop deposits and creating sedimentary models are important to understanding subsurface deposits (White and Willis, 2000; Fabuel-Perez et al., 2009; Butler and McCaffrey, 2010; Pickel et al., 2015; Burnham and Hodgetts, 2019; Marques et al., 2020; Sharifigaliuk et al., 2021) and can effectively promote hydrocarbon exploration and development (Maddy, 2002; Miall and Jones, 2003; Plink-Björklund and Steel, 2004; Enge et al., 2007; Fabuel-Perez et al., 2009; Hodgetts, 2013; Burnham and Hodgetts, 2019; Marques et al., 2020; Freitas et al., 2021; Janocha et al., 2021; Sharifigaliuk et al., 2021). In China, Qinghai Lake has been the subject of many detailed

Received May 25, 2022; accepted January 5, 2023

E-mail: lishunli@cugb.edu.cn

outcrops studies (Song et al., 2001; Qiang et al., 2013; Liu et al., 2016; Morgan and Craddock, 2017; Fielding et al., 2018; Moscariello, 2018; Yu et al., 2018a; Zhang et al., 2018b; Ding et al., 2019; Liu et al., 2019a; Liu et al., 2019b; Chen et al., 2020; Xue and Zeng, 2021). These studies have verified and improved upon the theories related to sedimentary systems in fluvial, and beach-bar systems (Zhang et al., 2018b; Wang et al., 2019a; Meng et al., 2020), and aeolian sedimentary models (Qiang et al., 2013; Chen et al., 2018; Ding et al., 2019; Liu et al., 2019b; Song et al., 2000; Xue and Zeng, 2021). Although previous studies have been conducted in this region, there has yet to be a detailed and comprehensive study on typical outcrop sections with the conversion process (Chen, 2016).

This study was performed on the Holocene Heimahe section, which is located on the southern shore of Qinghai Lake, China. The Heimahe delta has evolved from a single-provenance body with sandy and gravelly deposition to a multi-provenance mud-rich deposit. However, the sedimentary architecture, evolution stages, and controlling factors of this kind of delta have not been clarified. By means of field outcrop measurements, grain size analysis, and unmanned aerial vehicle (UAV) aerial photography (Paterson and Heslop, 2015; Yu et al., 2018a; Zhang et al., 2018a), 10 lithofacies and 7 lithofacies associations were identified. The sedimentary architecture, including 7 fourth-order and 4 fifth-order units, was also described.

This paper helps in understanding the sedimentary processes operating in a base-level cycle and proposes a depositional model considering the controlling factors. The purposes of this study are (i) to describe the sedimentary characteristics and spatial and temporal distribution of the delta in each stage and (ii) to discuss factors controlling the sedimentary evolution of the deposits in the outcrop. Furthermore, it can provide insights into the changes in the lake level variations of Qinghai Lake.

2 Geological setting

The study area is located on the north-eastern edge of the Qinghai-Xizang Plateau and south-west of Qinghai Lake, China (Fig. 1(a)). The Qinghai Lake Basin formed in the Pliocene, and lacustrine deposits formed at 0.5 Ma (Yuan et al., 1990). Typical deltaic sediments are present, and their provenance was the Nanshan Mountains in Qinghai (Chang et al., 2008). These sediments formed a multi-provenance delta with an area of 77 km^2 and an extension of 8 km (Figs. 1(b) and 1(c)). The study area is mainly composed of Quaternary deposits, and the lithology of the mountains to the south is mainly granitic (Fig. 1(d)). The study area has an inland plateau semiarid climate, with an average annual temperature of 0.8°C−1.6°C, an annual precipitation of 324.5−430 mm, and an annual evaporation of 1052 mm. The Heimahe River has a catchment area of 107 km^2 and an average runoff of 1×10^7 m^3. The surface of Qinghai Lake is at an elevation of the surface of Qinghai Lake is at an elevation of approximately 3194 m (Madsen et al., 2008).

2.1 Geologic structure

Before the uplift of the Nanshan Mountains, the Qinghai Lake Basin and Gonghe Basin were unified into “a single lake referred to as ancient Qinghai Lake” (Yuan et al., 1990; Bian et al., 2000; Lu, 2004; Madsen et al., 2008). In the Pliocene of the late Neogene, the movement of the Wenquan dextral strike-slip fault caused the reactivation of the northern Nanshan thrust fault, resulting in thrust faulting between the Gonghe Basin and the Qinghai Lake Basin and the uplift of the Nanshan range, which divided the ancient Qinghai Lake basin into the present Qinghai Lake Basin and the Gonghe Basin (Chang et al., 2008; Chang et al., 2009). This early tectonic activity involved shortening and continuous thrust faulting (Bian et al., 2000; Chang et al., 2009) (Fig. 1(d)).

The Nanshan Mountains are an arch-shaped mountain range that formed in the early Palaeozoic and is mainly composed of strongly deformed Triassic flysch and granite (Wang and Burchfiel, 2004). It is the western section of the large Qinghai Lake-Beihuaiyang Fault zone, which strikes WNW, dips SW, and has a dip angle of 50° to 70°. Data show that it is a normal fault along the southern margin of Qinghai Lake (Lanzhou Institute of Geology CAS, 1979). Qinghai Lake is the largest inland saltwater lake in China and is a typical fault-depression basin and an asymmetric rift lake that formed 2 Ma. The delta is developed on the deep regional fault zone at the southern edge of the Nanqilian Mountains, and its formation and evolution are related to tectonic movements of this major fault and climate fluctuations. The delta features a long asymmetric morphologic distribution. The periphery of the lacustrine basin is bounded by faults, which can be grouped into three main sets of fault structures with strikes of NNW, NW, and nearly N–S (Fig. 1(a)).

2.2 Regional stratigraphy

The Nanshan Mountains are mainly composed of Lower Triassic and Upper Carboniferous intrusive rocks. The lower part of the Triassic (T1) is dominated by dacite and rhyodacite, and the middle and upper parts are dominated by conglomerate and glutenite (Lanzhou Institute of Geology CAS, 1979; Yuan et al., 1990; Qinghai Bureau of Geology and Mineral Resources, 1991). The Heima River section was deposited during the Holocene.

The Neoproterozoic (N) Linxia Formation is characterized by a fine–coarse sedimentary sequence from the

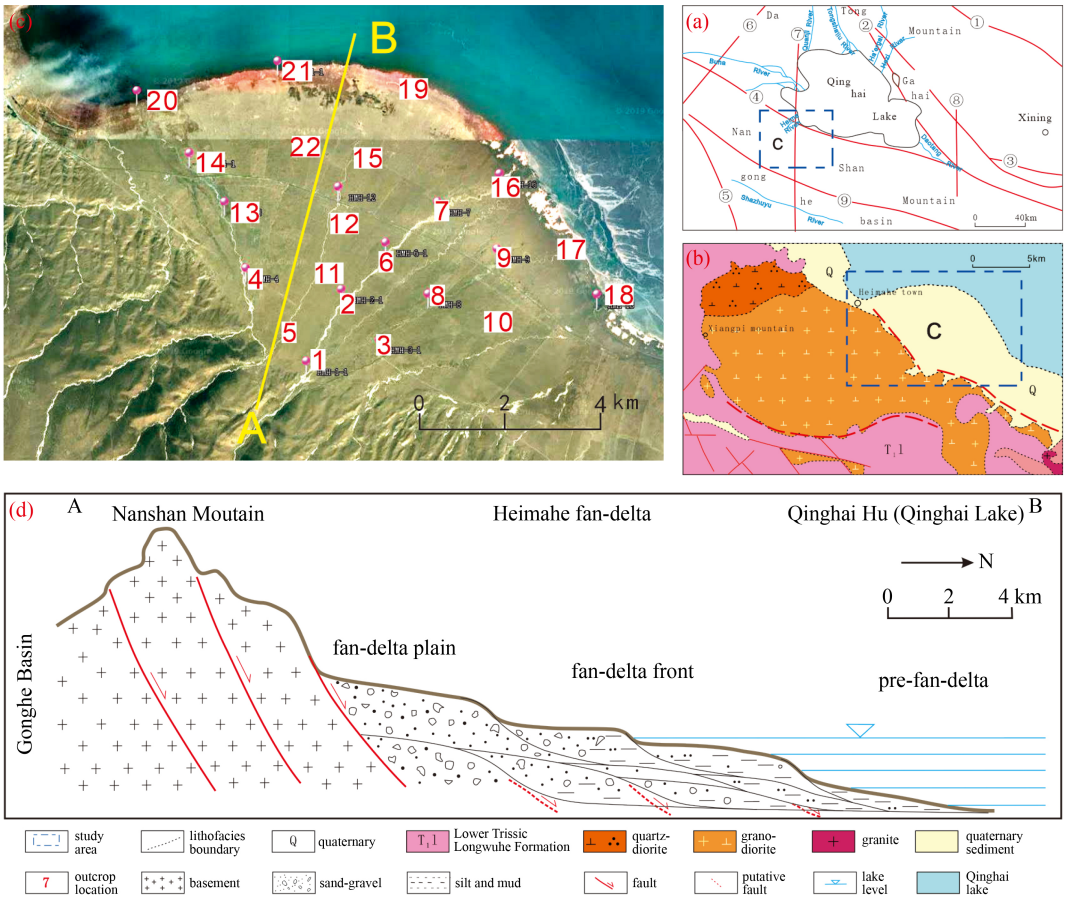

Fig. 1 Regional maps. (a) A schematic map of faults of Qinghai Lake area (modified from Bian et al. (2000)); (b) the outcrops location of the study area on satellite image; (c) lithology diagram of the study area and its surrounding area; (d) schematic section of the structure and sedimentation in the fan-delta, whose location was on (b) and (c).

bottom to the top, with two lithological sections, the upper and lower, and the two sections are in conformable contact. The rock assemblage of the upper section is interbedded dark gray multicomponent conglomerate and argillaceous silt. The dark gray multicomponent conglomerate and argillaceous silt are observed to alternate in the valley, are flat-lying, and are covered by Quaternary aeolian sand. The rock assemblage of the lower section (N2l1) is earthy yellow argillaceous siltstone mixed with brick-red silty mudstone and occasionally with fine conglomerate. The sedimentary structure of this section is characterized by parallel bedding and small cross-bedding, which reflects the weak overall hydrodynamic environment.

The lithology of the Quaternary (Q, including the Pleistocene and Holocene) strata is complex and diverse. The middle-lower Pleistocene (Qp1-2 gl + fgl) is a moraine deposit featuring a set of yellowish gray to brownish gray gravel layers with medium rounding, poor sorting, and low degrees of cementation. The Upper Pleistocene (Qp3al + pl) strata are the most widely distributed Quaternary deposits in the study area and consist of a set of gray gravel layers with silt and clay layers. The Holocene system is divided into a modern alluvial layer (Qhal) and a lake and marsh sedimentary layer (Qhh + l). The modern alluvial layer is mainly distributed in modern rivers or channels. The gravel layer is the main layer. The gravel is poorly sorted and weakly rounded due to the short transport distance, and there is no apparent structure. Lake and marsh sediments are distributed in modern shoreland areas and are rich in organic matter. These sediments are composed of bedded blue-gray to gray-black silt, mud, and clay and are rich in organic matter (Fig. 2) (Bian et al., 2000; Lu, 2004; Madsen et al., 2008).

3 Data and methods

The data sets used in this study were obtained from measuring and sampling 22 outcrop sections. The sections were described at decimeter-scale resolution. Grain size analysis and modern visualization techniques were also used (Paterson and Heslop, 2015; Blistan et al., 2016; Liu et al., 2016; Zhang et al., 2018a; Afuso and Matsubara, 2019).

Outcrops have the unique advantage of visualizing, specifying, and demonstrating the overall conditions in

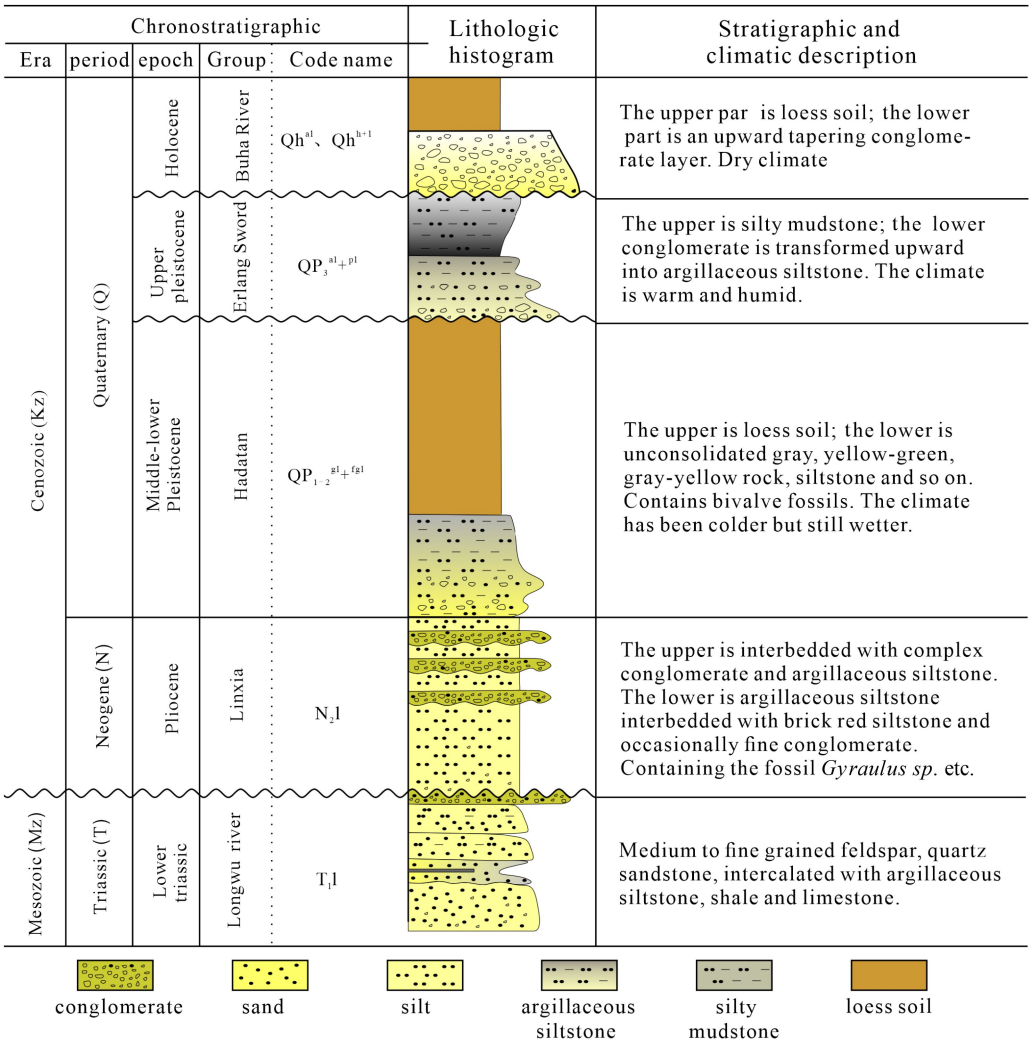

Fig. 2 A brief stratigraphic table of the Nanshan tectonic belt, Qinghai.

the study of sedimentary systems (Yu et al., 2013; Zhang et al., 2015; Shan et al., 2018). The location of each exploratory trench and outcrop was selected based on the following principles: 1) the section line distance was short, and the stratum was completely exposed; 2) unbroken stratigraphic sections were selected to the degree possible; and 3) sections formed by natural gullies or artificial excavation were fully utilized. In this study, a total of 22 outcrops in 6 lines (Fig. 1(c)) were selected from the outlet to the outer delta front, of which 2 trenches (measuring 1.5 m long, 1 m wide and 1.5 m deep) were excavated (HMH10 and 22 in Fig. 1(c)). A composite bar chart using a 1:10 vertical scale was drafted. Macroscopic photographs were taken to record the overall sedimentary characteristics of each point, and local zoomed-in photographs of special geological phenomena such as trough cross-bedding and macroscopic fossils were taken.

To characterize the sedimentary features of each profile, each location was sampled with a sampling density of 0.2−0.5 m and a sample weight of approximately 1 kg per sample. Basic information, such as sampling point, vertical depth and lithology, were recorded on the sample bag with a marker pen before analyzing the sample characteristics by sieve analysis. Grain size analysis was carried out by sieve (sifter). Each sample was disaggregated into its component grains, which were separated into eight fractions according to the amount of sample passing through a set of pore sizes (−1.6ϕ, −1ϕ, 0ϕ, 1ϕ, 1.3ϕ, 2ϕ, 3ϕ, and 4.5ϕ). Each of the eight fractions was weighed, and the amount of each as a portion of the total weight was calculated. Subsequently, the corresponding cumulative percentage was calculated, and then a cumulative frequency curve, which can reflect the hydrodynamic conditions during deposition, was generated.

The elevation data were obtained through satellite systems. The application of unmanned aerial vehicle (UAV) aerial photography technology is becoming increasingly widespread, and its use in field outcrop research is becoming common (Enge et al., 2007; Afuso and Matsubara, 2019). This technology can easily achieve

the goal of recording the overall characteristics of the research target. This study used a DJI UAV M200 to take multiple sets of photos at 50 m, 80 m, and 100 m from the ground.

4 Sedimentary characteristics

4.1 Lithofacies and architectures

4.1.1 Lithofacies identification

Since sedimentary structures in gravels are not well developed and the grain size and support forms of clasts are complex and diverse, a single lithology or sedimentary structure cannot accurately reflect the depositional environment (Ghazi and Mountney, 2009; Trendell et al., 2013; Zhang et al., 2015; Tan et al., 2017; Shan et al., 2021). Lithofacies types were identified by integrating key factors, including grain size, sedimentary fabrics, and sedimentary structures, with detailed field outcrop observations and descriptions according to the principle of origin-structure classification (Fig. 3).

4.1.1.1 Gravelly facies

1) Multigrade clast-supported, massive gravels (Gmc)

This lithofacies is characterized by light gray to gray boulders, cobbles, pebbles, and granules mixed with sandy and muddy sediments. The gravel clasts are mainly composed of granite and metamorphic clasts, with diameters of 5 cm to 50 cm and a maximum of 1.5 m. The gravel clasts are poorly sorted with medium roundness, exhibiting multigrade clast-supported features with plenty of sandy and muddy matrix. The Gmc shows massive, chaotic characteristics and contains rare clasts with high dip angles (> 70°). This type of lithofacies is generally thick bedded with thicknesses generally over 30 cm to 50 cm. The massive, multigrade straight gravel clasts indicate that this lithofacies was typically developed by high-density debris flows, which were triggered by intermittent flood events. The debris flows were generally characterized by high viscosity and cohesion, transporting large volumes and chaotically oriented clasts (Zhao et al., 2015).

2) Clast -supported, imbricated gravels (Gic)

This kind of lithofacies mainly consists of gray pebbles with granules and pebbles. Most of the pebbles are elongated with axial lengths from 3 cm to 8 cm and show imbricated structures with low dip angles (commonly less than 30°). In the field trench profiles, multiple stories of clast-supported, imbricated gravels dipping upstream with respect to the river are observed. Each individual layer of Gic shows medium sorting and roundness with thicknesses of approximately 10 cm to 15 cm. However, the average diameter of the gravel clasts and thickness of each layer varied among the different layers in the vertical profile. The clast-supported, imbricated gravels of this flat facies indicate dilution of the high-density debris flows, which transformed into sheet flood currents (Galloway, 1996). This type of lithofacies is a product of transformational flows, which exhibit sedimentary textures and structures typical of both debris and traction flows (Ghazi and Mountney, 2009).

3) Matrix-supported, massive graves (Gmm)

This lithofacies is characterized by gray pebbles, cobbles, and yellowish gray fine-grained sands. The gravels mainly consist of granite clasts with diameters from 5 cm to 10 cm and a maximum of 25 cm. The gravel clasts are poorly sorted and well rounded, and they are supported by a fine-grained sandy and muddy matrix. The Gmm generally shows massive characteristics without any structures. In the outcrop section, the gravel clasts appear to float in the matrix, and the layers range in

Code	Gmc	Gmm	Gcc	Gic	St	Sp	Sh	Sm	Fm	Fl
Name	Gravel-supported floating conglomerate facies	Sand-supported floating conglomerate facies	Multi-stage particle supported conglomerate facies	Imbricate conglomerate facies	Trough cross bedding sandstone facies	Planar cross bedding sandstone facies	Parallel bedding sandstone facies	Massive sand facies	Massive silt facies	Massive mud facies
Description	Medium and coarse gravels float on medium and fine gravels;Poorly sorted and rounded; Vertical gravels are found.	Gravels float on sand;Poorly sorted and rounded;Vertical gravels are found.	Medium coarse gravel filled with fine gravel and sand;Poorly sorted and rounded;Vertical gravels are found.	Medium-fine gravel;Gravels oriented along the striations; Poor sorted, medium-rounded; Sand-based support	Gravel-bearing medium and coarse sand; Fining upward; Trough cross bedding.	Medium-coarse sand; Medium-poor sorted; No obvious grain sequence; Planar cross bedding.	Mainly medium-coarse sand; Medium-poor sorted; No obvious grain sequence; Parallel bedding.	Massive sand without obvious sedimentary structure	Massive silt without obvious sedimentary structure	Massive mud without obvious sedimentary structure
Genetics	Non-Newtonian fluid; High-density sediment gravity flow; Coarse gravels supported by fine gravels and transported by suspension	Non-Newtonian fluid; High-density sediment gravity flow; Gravels supported by coarse sand and transported in suspension	Non-Newtonian fluid;High-density sediment gravity flow; Multi-stage particle supported	High-density torrent; imbricate gravel	Traction flow; Incised filling of the river	High laminar flow	High laminar flow	Low laminar flow	Low energy environment	Steay water
Lithofacies	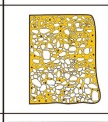		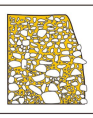			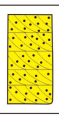				
Picture			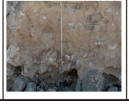						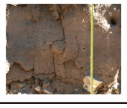	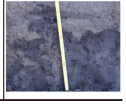

Fig. 3 Lithofacies of the Heimahe delta deposites.

thickness from 15 cm to 30 cm. The high content of sandy or muddy matrix of this lithofacies suggests dilute debris-flow deposition with a relatively low density and concentration of sediments, likely left by local failures or sandy cohesionless debris-flows (Shan et al., 2021).

4) Clast-supported, cross-bedded gravels (Gcc)

This lithofacies is mainly comprised of gray, relatively fine-grained clasts dominated by pebbles and granules with coarse-grained sands. The diameters of the granules in this lithofacies are commonly less than 3 cm. Most of the gravel clasts are well rounded and medium-to-well sorted. In the outcrop trench profile, trough planar cross-bedding is observed in the Gcc facies. Gravel clasts on the bedding surfaces occasionally show imbricated features. The thicknesses of these clast-supported, cross-bedded gravel beds range from 10 cm to 50 cm. Cross-bedding of the sediments in this lithofacies indicates that the dominant depositional agents were traction currents, which generally form during the attenuation of floods. However, the gravelly sediments suggest the flows still exhibited strong hydrodynamics (Miall, 1985).

4.1.1.2 Sandy facies

1) Trough cross-bedded sands (St)

This lithology is dominated by brownish gray gravel-bearing coarse- and medium-grained sands with fining-upward sequences, and the clasts are well sorted and rounded. Trough cross-bedding is well developed, and the beds range in thickness from 10 cm to 30 cm. Granules generally occur at the base of the trough cross-bedding, which commonly show erosive features. Groove-like structures forming a downward concavity in the sandy layers, which are a typical sedimentary structure of traction flows under high-energy conditions, reflect the downcutting and filling of channels (Miall, 1985).

2) Planar cross-bedded sands (Sp)

This facies is characterized by the predominance of gray, medium- and coarse-grained sands with high roundness and good sorting. The planar cross-bedding generally exhibits blocky or weak coarsening-upward sequences with thicknesses ranging from 5 cm to 15 cm and lateral continuity of up to tens of meters. This facies is characterized by the sedimentary structure formed by the tangent of the laminae formed by water eroding the top of a previously deposited layer followed by lateral or vertical accretion of bedforms (Miall, 1985; Wang et al., 2019a).

3) Parallel-bedded sands (Sh)

This facies mainly consists of fine- and medium-grained sandy sediments with parallel bedding. This thin-bedded lithofacies generally exhibits flat tops and bases with thicknesses ranging from 5 cm to 25 cm, and these layers feature good later extents and no obvious cross-stratification. Rare granules are distributed at the base of the bedding. This facies reflects the presence of rapid, high-velocity traction currents, representing the transition from subcritical to supercritical conditions resulting in the deposition of sandy facies during stages of decreasing current strength (Yu et al., 2013).

4) Massive sandy facies (Sm)

This facies is characterized by a blocky structure of medium- to coarse-grained sandy deposits, containing a small amount of fine-grained gravel. The bases of this facies are generally flat or slightly irregular, without obvious vertical grading. This facies is generally thick bedded (up to 50 cm) with lenticular shapes in lateral extent. This massive sandy facies indicates sustained, highly concentrated floods that transported large volumes of sandy sediments in a short time, resulting in high rates of deposition (Yu et al., 2013).

4.1.1.3 Muddy facies

1) Massive muddy facies (Fm)

This facies mainly consists of brownish gray, structureless mud and silt with rare floating granules. Plant roots are generally developed at the top of this muddy facies. The thickness of the massive muddy facies varies in different locations, ranging from 10 cm to 70 cm. This fine-grained facies formed through the deposition of suspended sediments under relatively stable hydrodynamic conditions. However, the thick-bedded vertical feature indicates a high rate of sedimentation associated with dilute floods (Miall, 1985; Fabuel-Perez et al., 2009).

2) Laminated muddy facies (Fl)

This facies is characterized by gray to dark gray, clay-dominated sediments. In the vertical direction, clayey sediments exhibit subtle color changes or are interbedded with silty layers, resulting in laminations with thicknesses ranging from less than one millimeter to a few millimeters. This facies is commonly developed with fine-grained sands showing wide lateral continuity. The laminated muddy facies indicate suspension-dominated deposition under a low hydrodynamic environment with a low rate of sedimentation (Miall, 1985).

4.1.2 Lithofacies association and architectural elements

The characteristics of lithofacies associations are an important indicator for determining the genesis of coarse-grained sediments (Tan et al., 2017; Li et al., 2018; Yu et al., 2018b; Fu et al., 2020; Shan et al., 2021). The architecture units proposed by Allen (1983) have been used as an important mean to identify sedimentary facies. According to the six-level interface classification proposed by Miall (1985) and the principle of architecture classification (Miall, 2002; Deynoux et al., 2005; García-García et al., 2006; Backert et al., 2010; Yu et al., 2018a), the architecture units has been refined in the field. Based on the description and lithofacies identification, seven

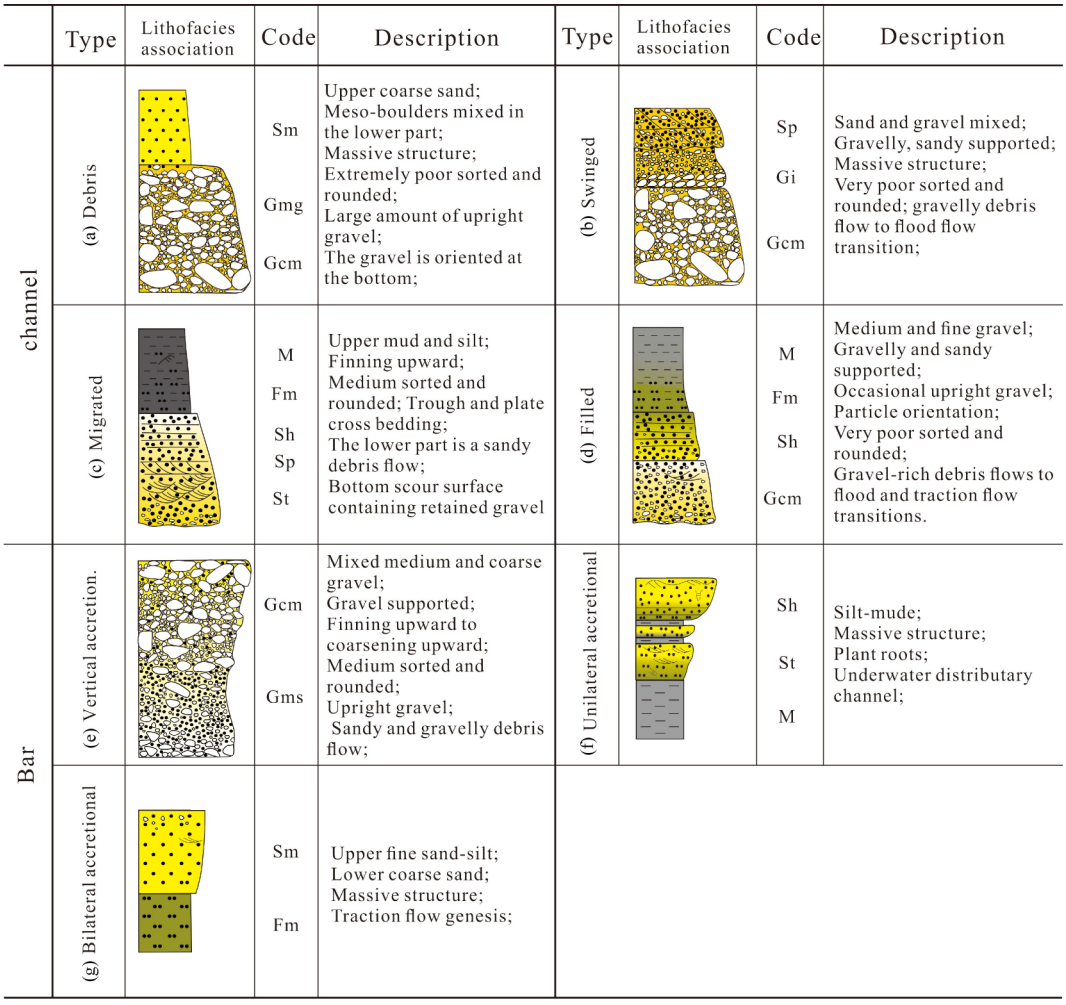

Fig. 4 Typical lithofacies associations of the Heimahe delta.

major vertical sequences (Fig. 4), namely, architectural elements (Fig. 5), were determined. To clarify the sedimentary characteristics and distribution patterns of different subfacies, the morphology of sedimentary bodies was dissected, and the macroscopic variation patterns of delta sand and gravel bodies were studied.

4.1.2.1 Channel

1) Debris-flow channel (CHd)

It shows the development of thick-bedded, coarse gravel deposits dominated by Gmc and Gmm with Sm. The channel is mainly composed of matrix-supported, poorly rounded, and poorly sorted gravel. The maximum gravel diameter in the profile can reach 26 cm, and the maximum grain size seen in the channel reaches 147 cm. Occasional larger gravel clasts have a floating or straight-up distribution and blocky structure. The clasts are poorly sorted and are supported by a poorly sorted matrix of sand, silt, and mud. Beds of these lithofacies have a sharp interface but no erosional relationships with the underlying beds.

A debris-flow channel is created by highly concentrated flows and generally show blocky or weak normal grading. These data reflect the debris-flow deposits containing mixtures of gravel, sand, and mud on the steep slope of the proximal area (Zielinski and Gozdik, 2001) (Figs. 4(a) and 5(a)).

2) Switched channels (CHs)

Switched channels are characterized by an obvious fining-upward pattern, with poorly sorted and coarse-grained multistage supported gravel facies (Gmc) at the bottom, transitioning upwards to a finer-grained sandy supported gravel facies (Gmm), and a directionally imbricated gravel facies developed at the top. From the bottom up, the gravel directionality gradually increases, the bottom often features a scouring surface, the top is a gradational contact, and various interlacing laminations are developed. It is dominated by trough-like interlacing laminae and grain-order laminae, with a gradual upward-fining trend.

Large flood events and downstream aggradation are the main controlling factors of CHs. This association is the product of the formation of distributary channels after the

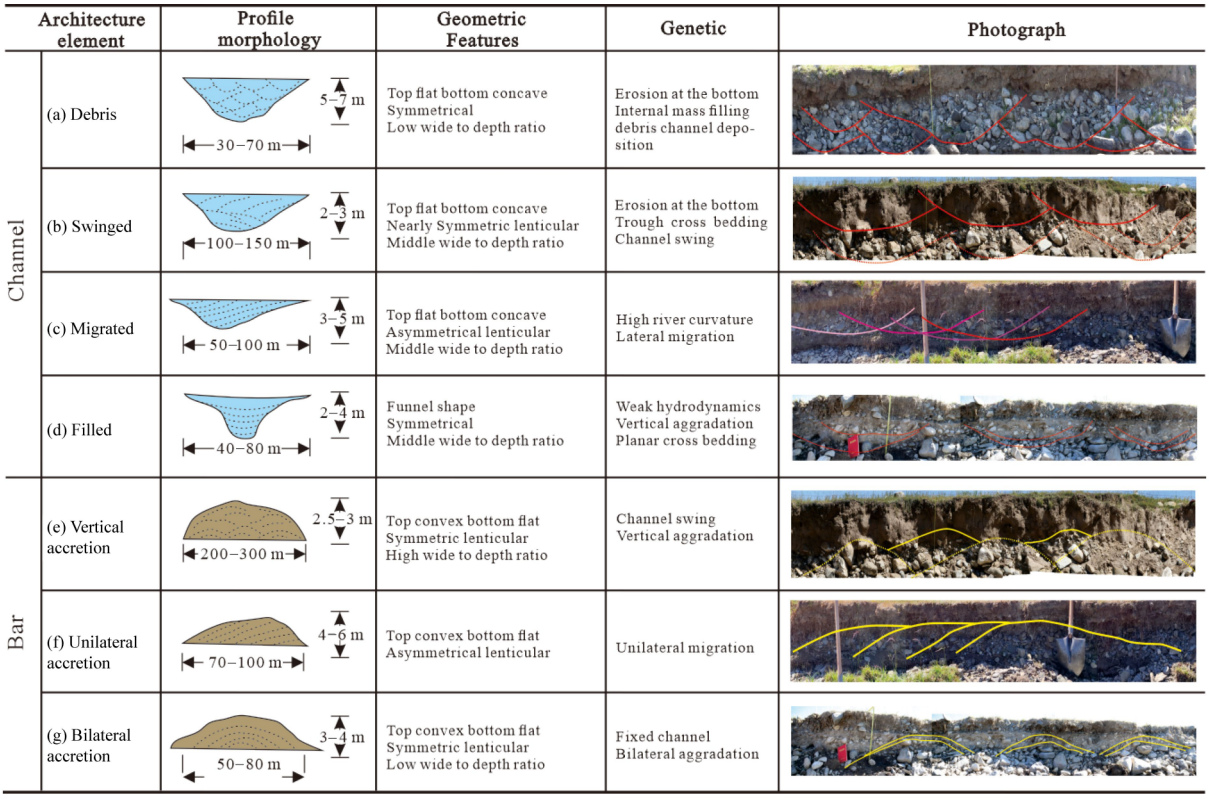

Fig. 5 Characteristics of the architecture elements. (a) Debris-flow channel (CHd); (b) Switched channels (CHs); (c) Migrated channel (CHm); (d) Filled channel (Chf); (e) Vertical accretion (Bv); (f) Unilateral accretion (Bl); (g) Bilateral accretion (Bb).

unloading of suspended materials in the debris-flow channels and the reduction in viscosity. The transition from a debris-flow to a traction flow is consistent with the development of bilateral accretionary bars (Zielinski and Gozdik, 2001; Ghazi and Mountney, 2009) (Figs. 4(b) and 5(b)).

3) Migrated channel (CHm)

The lithofacies of Gmc, St, Sp, Sh, and Fm constitute the CHm element. The facies is dominated by medium-coarse-grained silt and sand. Fining-upward sequences are developed, and the thickness of trough cross-bedded sand layers is thin, topped by a thin imbricated lateral accumulation, parallel lamination or block structure (Figs. 4(c) and 5(c)). The laminations mostly converge in the same direction.

The planform of CHm consists of unitary lateral migration in channels due to some unidirectional lateral aggradation bedforms. The smaller size of the cross-beddings reflects the weakening of the hydrodynamic force, and the parallel bedding at the top indicates the rapid reduction in the particle size transported. This type of channel develops in a meandering river at the distal end of the fan (Ghazi and Mountney, 2009; Li et al., 2015a).

4) Filled channel (CHf)

This association shows a complete gravel–sand–mud sequence in the vertical direction, and the lithology is gravelly sand and coarse sandstone. The bottom is characterized by a multigrade clast-supported gravel facies (Gmc) with a small grain size, and the top is a parallel-laminated fine sand stage (Sh), massive mudstone (Fm), and laminated mudstone (Fl). Fine-grained sand is the main lithology. The scale of the trough cross-bedding in this association is smaller than that in channels. Scouring surfaces are found at the base of the CHf.

The fine-grained sediments suggest that the CHf formed following the rapid reduction in energy after high-speed water flowed into a lake (Olariu and Bhattacharya, 2006; Li et al., 2015a) (Figs. 4(d) and 5(d)).

4.1.2.2 Bars

1) Vertical accretion (Bv)

This association shows an obvious upward-coarsening trend, with a sandy matrix base supporting gravel facies at the bottom and multistage particles supporting gravel facies at the top, with a gradual decrease in the matrix content from the bottom to the top. The cyclicity is not obvious and is mostly blocky. The basal contacts of Bvs are usually erosive. Downward-climbing cross-bedded sets rest on significant erosion surfaces. Planar cross-bedding is well developed, some clasts are imbricated, and the intergranular expression is multilevel granular support. Some channel elements are developed in the Bv elements.

Similar to the switched channels, this association represents the transition from debris flow to traction flow.

During this depositional process, the hydrodynamic conditions gradually weaken and stabilize, sediment slowly deposits, and the sediment body gradually grows (Olariu and Bhattacharya, 2006; Wakefield et al., 2015) (Figs. 4(e) and 5(e)). There is no trough cross bedding reflecting vertical accretion.

2) Unilateral accretion (Bl)

The lithofacies of this association vary markedly and mainly include St, Sp, and Sh. This association shows a wide range of grain sizes, with gravel, sand and silt all being present and exhibiting a typical upward-fining trend. There is trough/planar cross-bedding at the bottom, small trough cross-bedding and climbing cross-bedding in the middle and upper parts, and horizontal laminae can be seen at the top. The lamination downlaps onto the channel floor.

The bedding is formed by the continuous lateral migration of the channel and the weakening strength of the bottom flow (Li et al., 2015a; Wakefield et al., 2015) (Figs. 4(f) and 5(f)). Bl is often deposited in high-sinuosity channels associated with CHm and CHt.

3) Bilateral accretion (Bb)

Bb is interpreted as the downstream and bilateral accretion of compound bars based on the internal arrangement of accretion surfaces (Maill, 2014b). Large-scale Sp sets associated with downstream-oriented flow are abundant. This association features fine sand and silt dominated by anti-grain order in the vertical direction. The clasts are relatively well sorted and rounded. On its flanks, a slotted interlayer formed by channel scouring is visible, and parallel laminae are developed at the top

It is possible that accretion can occur at the downstream end of a channel bar from DA elements. This represents the accretion of sediments carried by the channel inlet (Ghazi and Mountney, 2009; Li et al., 2015a) (Figs. 4(g) and 5(g)).

4.2 Architecture stacking pattern

The Heimahe Delta, which developed in the steep slope zone of this lake, is characterized by a proximal sediment provenance, coarse-grained and poorly sorted sediment, strongly heterogenetic features, complex internal structures, and mixed sedimentation styles. The analysis of individual outcrop profile characteristics reveals obvious differences and regular features (Ghazi and Mountney, 2009; Li et al., 2014, 2015b; Wakefield et al., 2015).

4.2.1 Debris-flow channel (D)

Debris-flow channels (Fig. 6(a)) are distributed in the upper delta plains, are formed by the cutting and stacking of debris-flow channels during flood stages, and are dominated by debris flows. Due to the proximity to the provenance area and the steep topographic slope, the flowing water carries a large amount of mud, sand, and gravel during the flood stage, which intensely scours pre-existing deposits and accumulates rapidly in the channels, forming gravel with matrix support. These deposits have low textural and compositional maturity, high gap-fill content, and large volumes. As the flood subsides and energy weakens, the debris flow gradually transitions to a sheet flow, the matrix content decreases, and gravel deposits dominated by granular support form on top of the previous stage in the debris flow channel. In the next flood stage, new debris-flow channels cut into and erode the previous channel deposits, and there is no obvious pattern in the superposition relationship (Shan et al., 2018).

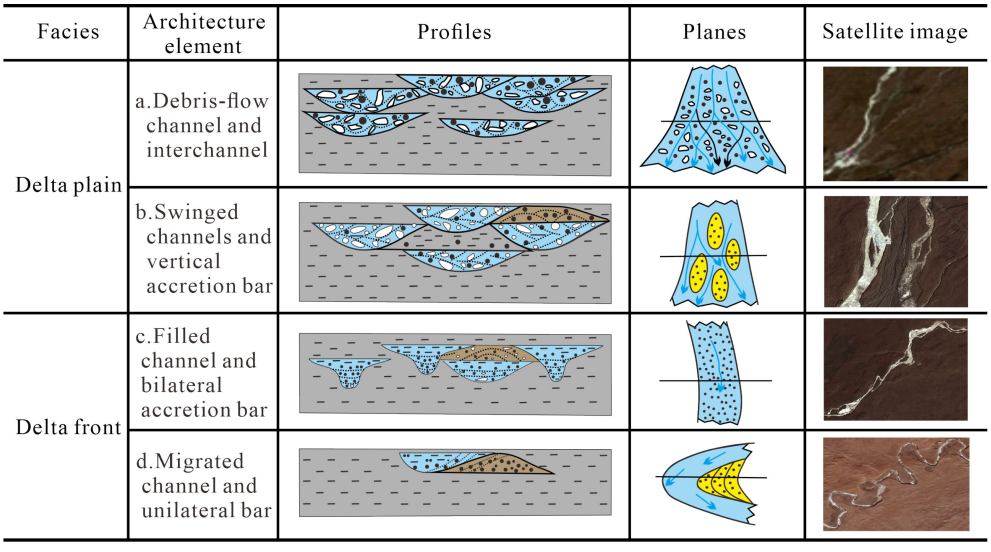

Fig. 6 Characteristics of the architecture stacking pattern. (a) Debris-flow channel and interchannel (D); (b) Switched channels and vertical accretion bars (S); (c) Filled channels and bilateral accretion bars (F); (d) Migrated channels and unilateral accretion bars (M).

4.2.2 Switched channels and vertical accretion bars (S)

S is mainly developed in the lower delta plain, and the most common superimposed assemblages are those of channel channels and channel bars. With the unloading and accumulation of a large amount of debris material in the plain during the flood stage, the energy and density of the fluid weakens after entering the lower delta plain (Zhang et al., 2015). The sediments are coarse-grained gravels, but the traction flow dominance is more pronounced. Gravel is carried and deposited mainly as bottom loads, resulting in more and smaller bifurcations in the switched channels and the beginning of vertical accretionary bar development. The lithology of the bar body is mainly gray sandy fine gravel and medium gravel, and the cyclicity is not obvious and is mostly blocky. The channels are mostly lateral and superimposed on each other and on the bar, reflecting the switched nature of the channels (Ghazi and Mountney, 2009); isolated channels can also be seen (Fig. 6(b)).

4.2.3 Filled channels and bilateral accretion bars (F)

F is mainly formed by the filled submerged distributary channel and bilateral accretion bars. This reflects the depositional characteristics of gradually weakening hydrodynamics and decreasing sediment supply during deposition. This lithofacies association is dominated by gray and dark gray sandy fine gravel deposits, which are finer in grain size than the above assemblage. The vertical direction exhibits a fining-upward trend, with the bottom being the erosional scour surface of the channels, while the top is in gradational contact with the overlying deposits (Ghazi and Mountney, 2009) (Fig. 6(c)).

4.2.4 Migrated channels and unilateral accretion bars (M)

M is mainly distributed at the delta front and are dominated by migratory channels and unilateral accretion bars. The lithology is mainly gray, greenish–gray or dark gray siltstone and mudstone. There is composite bedding, small-scale sand bedding and horizontal bedding, with fining-upward or homogeneous characteristics in the vertical direction. This lithofacies association represents the fine-grained sedimentary part of the delta sedimentary system with a high degree of channel curvature and frequent distributary channels (Tunbridge, 1981; Olariu and Bhattacharya, 2006; Li et al., 2015a) (Fig. 6(d)).

4.3 Sedimentary distribution

4.3.1 Delta plain

The proximal end of the upper delta plain is dominated by thick-bedded boulder gravel and coarse gravel with low matrix content and consists of multiple stages of debris-flow channel (D) deposits superimposed by vertical upwards scouring, with a one-stage cumulative probability curve (Yu et al., 2013; Li et al., 2015a) (Fig. 7(a)). The scouring surfaces at the bottom of the debris-flow channels are strongly convex downwards, and a large amount of boulder gravel is visible, transitioning upwards to medium and coarse gravel, with sandy or gravelly matrix supporting the floating gravel facies, with very poor sorting and rounding (Fig. 7(b)). The bottom of the second stage is superimposed by a multigrade debris-flow channel or switched channel (S) scouring, with a flat top and convex bottom, transitioning upwards to grain-supported, poorly sorted and rounded medium gravel with a sandy matrix. The profile shows a gradual decrease in gravel grain size from bottom to top, a decrease in single-bed thickness, a decrease in the degree of scouring of the channel, and a transition from multistage superposition to sheet floodplain in the vertical direction (Fig. 7(c)). This pattern reflects the gradual migration of the fan with the migration of the accommodable and the change in the magnitude of the sediment supply during development. The top three stages are massive chalky sands, representing low-flow diffuse deposits when hydrodynamic conditions weaken (Fig. 7(d)).

The lower delta plain features smaller grain sizes. The lower part is debris-flow channel (D) deposits, dominated by fine gravel and medium-coarse sandstone, supported by multigrade grains, occasionally with upright gravel clasts or gravel clasts arranged in a high-angle orientation (Zhao et al., 2015) (Fig. 8(a)). The middle of the profile has a high-porosity nature. The unstable distribution of S is caused by the flushing of loose fine-grained deposits that have not been consolidated by the later continuous flow (Fig. 8(c)). The upper part is a debris-flow and migrated channel with unilateral accretion bar (M) deposits, no obvious sedimentary structure, sand-rich debris-flow to traction current deposits, and a cumulative probability curve indicative of a transition (Fig. 8(d)).

4.3.2 Delta front

The delta front mainly features filled channels and bilateral accretion bars (F) and migrated channels and unilateral accretion bars (M).

During the downward flow of the distributary channel, a filled channel (F) is gradually formed due to the further reduction in hydrodynamic conditions and the flattening of the topographic area. Migrated channels develop near the delta front (Fig. 9(a)). The early water column was more energetic with strong energy at the time of bottom deposition in the delta plain. The sandy matrix content is greater in Gmc and mainly a mixture of medium sandstone and gravel. The local sandy matrix content can be greater than 70%, characteristic of debris-flow (D) deposits (Fig. 9(b)). Due to the lake transgression in the middle stage, the profile shows a clear rapid upward grain

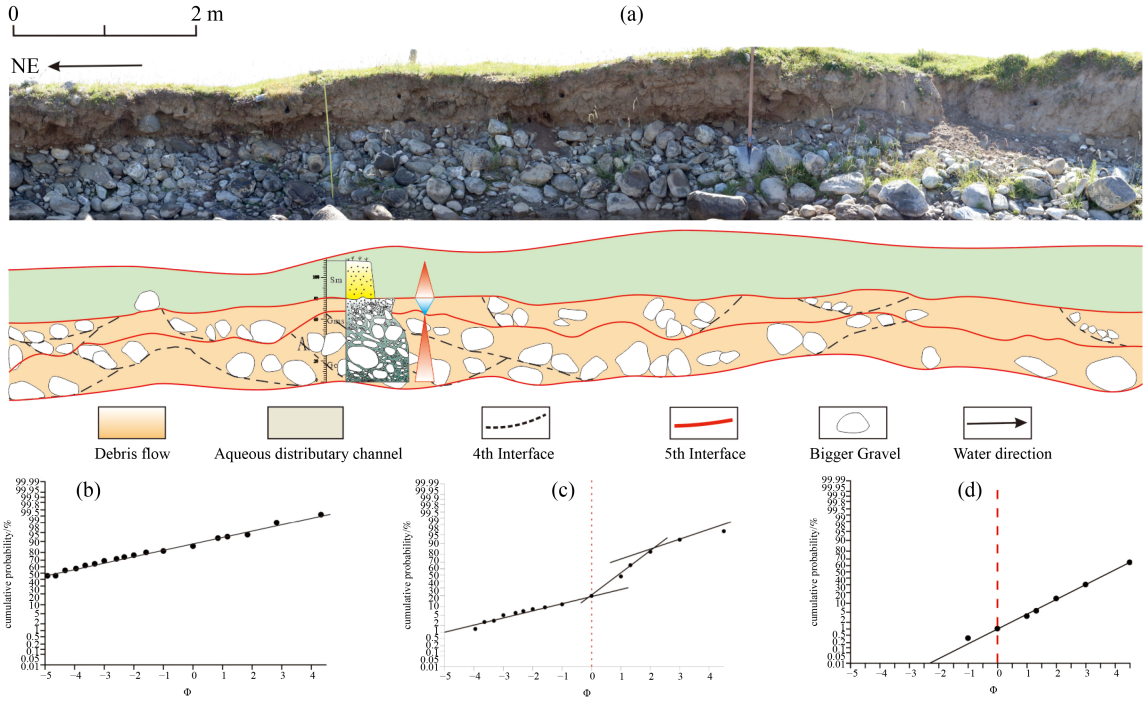

Fig. 7 Panoramic photo, interpretation for outcrop profile 1(location in Fig. 1(c)) of the lower delta plain and cumulative probability curves of three deposition stages. (a) Panoramic photo of outcrop profile 1; (b) cumulative probability curve for firste-stage; (c) cumulative probability curve for second-stage; (d) cumulative probability curve for third-stage.

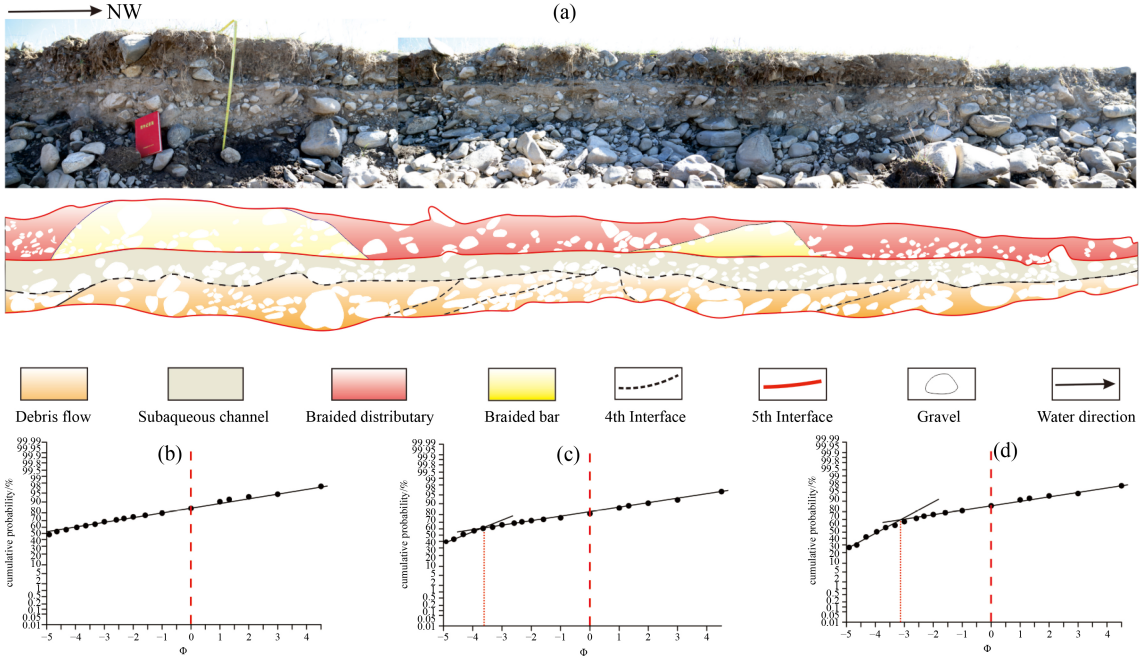

Fig. 8 Panoramic photo, interpretation for outcrop profile 14 (location in Fig. 1(c)) of the lower delta plain and cumulative probability curves of three deposition stages. (a) Panoramic photo of outcrop profile 14; (b) cumulative probability curve for firste-stage; (c) cumulative probability curve for second-stage; (d) cumulative probability curve for third-stage.

size reduction to silt, and overflow deposits are observed (Li et al., 2015a) (Figs. 9(a) and 9(c)). Traction current (Fig. 9(d)) deposits are present at the top of the profiles.

During the downward flow of the distributary channel, filled channels and bilateral accretion bars (F) are gradually formed due to the further reduction in hydrodynamic conditions and the flattening of the topographic area (Yu et al., 2018a) (Fig. 9(a)).

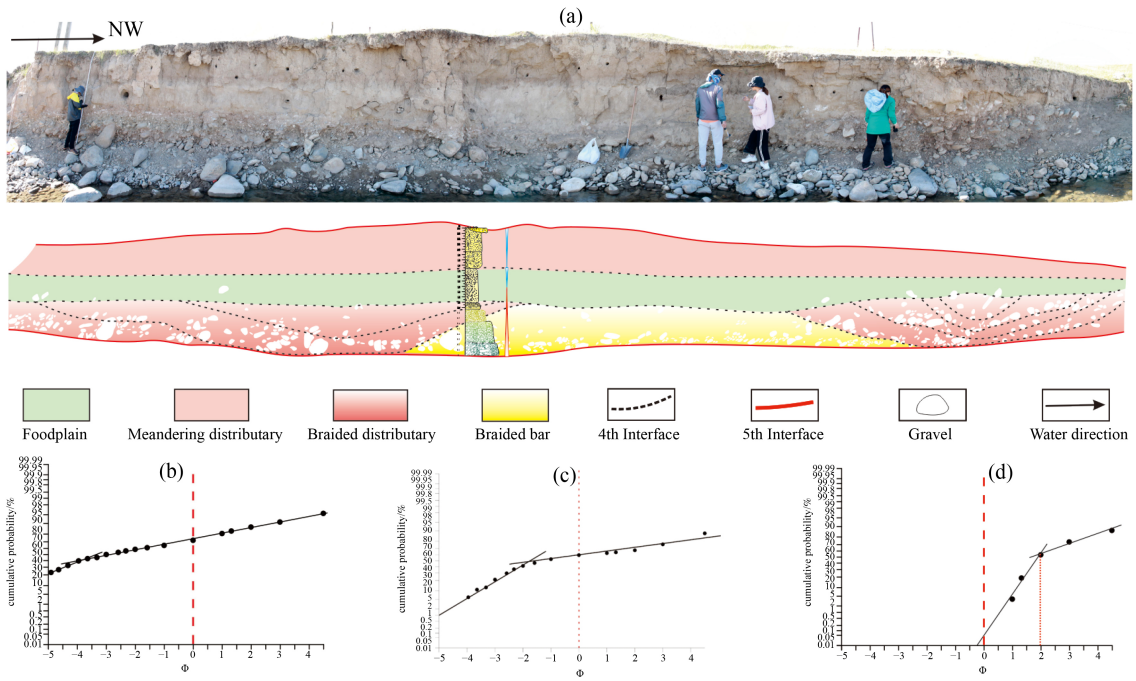

Fig. 9 Panoramic photo, interpretation for outcrop profile 7 (location in Fig. 1(c)) of the delta front and cumulative probability curves of three deposition stages. (a) Panoramic photo of outcrop profile 7; (b) cumulative probability curve for first-stage; (c) cumulative probability curve for second-stage; (d) cumulative probability curve for third-stage.

5 Discussion

5.1 Evolution stages

Detailed depiction of field outcrops and grain size analysis were the main data used for this study, and detailed profile 7 (Figs. 1(c) and 9) served as an important basis for stage analysis. The bottom of the lower section exhibits gray to greyish-yellow medium to coarse gravel, and the underlying strata could not be observed. The top has an abrupt lithologic change surface with no obvious sedimentary structure, but there is an obvious gravel orientation arrangement that tends to the south, and occasional upright gravel clasts can be seen. The gravel clasts are mainly composed of granite and gneiss, have grain sizes of 3 to 12 cm (locally up to 1 m) (Fig. 10), are characterized by poor sorting and poor to medium rounding (Figs. 11(a) and 11(b)), and are present in the flood-stage delta distributary channels. The transport mechanism of these clasts is debris flows (Tanaka and Maejima, 1995; Ulicny, 2001; Wu et al., 2010). Most of the medium to fine gravel and all the coarse gravel were unloaded onshore as the lake level rose rapidly during flooding of this area. The distributary channel acts as a dominant channel for transporting gravel and exhibits top gravelly sandstone deposits (Figs. 11(a) and 11(b)), representing the transitional stage from a debris flow to a traction flow (Fig. 11(c)). The histogram shows rapid upward grain size reduction and disappearance of gravel grains in this section, indicating a rapid rise in lake level. The middle section is a thick greyish yellow layer of gravelly fine sand, silt, and muddy silt, which are in sharp contact with the underlying gravel. Abundant white bioclastic (Figs. 11(d) and 11(e)), reed-related tufas formed by a calcareous wreath attached to the base of the trunk (Fig. 11(f)), a few intact fossils (Figs. 4(g)–4(i)), and burrows with backfilling structures (Figs. 11(j) and 11(k)) are present in the lower part. Many root-lap structures (Fig. 11(l)) are seen in the middle and upper parts. These findings indicate that this was the location of the lake shoreline at the time, with shallow water depths and fast deposition rates, and that the deposition boundary between each flood stage was not obvious due to strong wave modification. The profile shows the darkening of the upper part and the abundance of root-lap structures, and the overall grain order is not obvious (Fig. 10) (Wu et al., 2010; Yin et al., 2020). However, the observations reflect the shallowing of the water, characterized by thickly bedded gray–brown silt and fine sand with no obvious change in grain size. The increase in root-lap structures also indicates that the water became shallower as the lake level fell, and small-scale gravel-filled washes developed at the top because of the last decline in the lake level. The existence of multiple terraces on the surface is also proof that the lake level rapidly declined (Fig. 12).

Correspondingly, there are three stages. The first stage is the progradation to aggradation (PA) (Neal and Abreu, 2009) stage (Fig. 13(a)), which is characterized by gravel-rich sedimentation. The sedimentary characteristics of

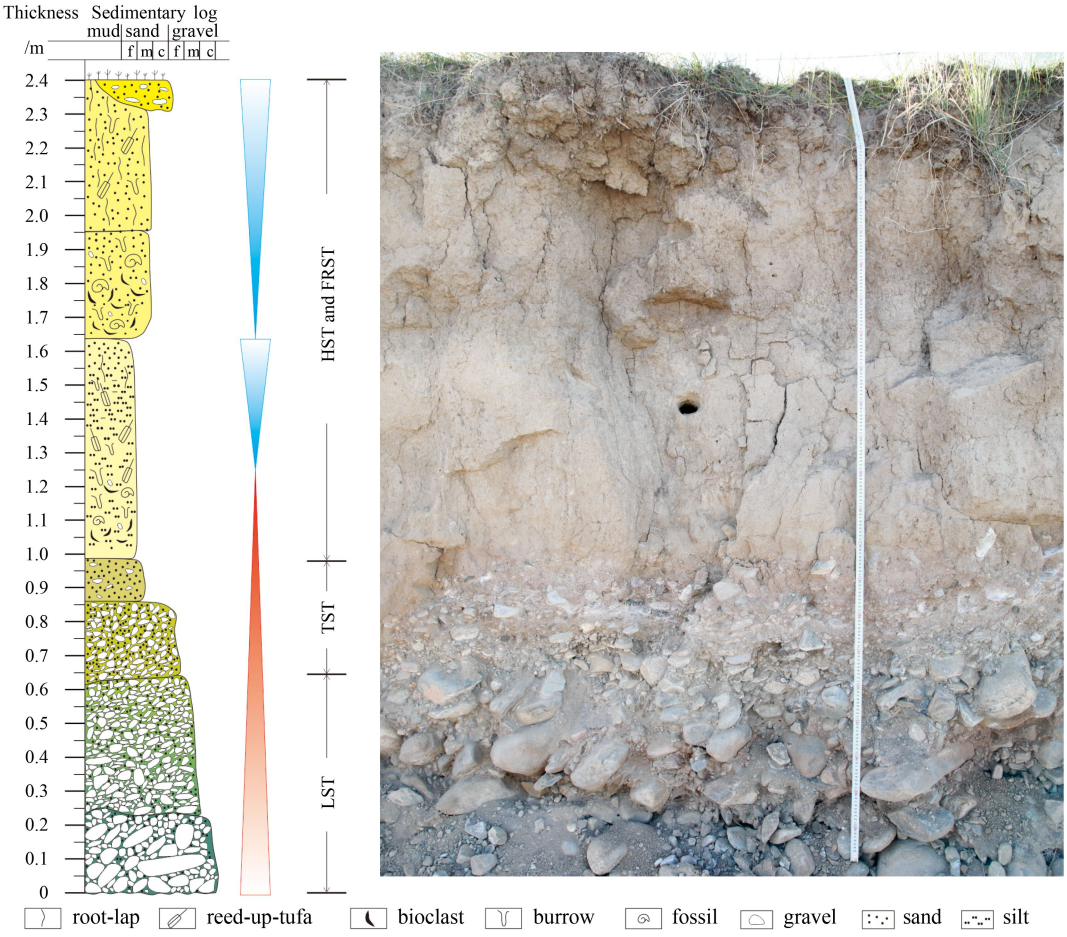

Fig. 10 Deposional cycles and panoramic photo for outcrop profile 7 (location in Fig. 1(c)).

this stage are similar to those of most deltas, and the channels are dominated by debris-flow channels and switched channels. The stacking pattern is S type with high-angle deposits, and the sedimentary center is in the middle of the delta plain (Fig. 14, Stage I). This stage developed through cut-and-stacking and continuous deposition and was dominated by coarse-grained deposition with low textural and compositional maturity. The thickness is thick, the grain size is coarse, most sediment is from a single provenance, and no vegetation developed. The second stage is the lacustrine transgressive system, i.e., the retrogradation (R) (Neal and Abreu, 2009) stage (Fig. 13(b)). Deltaic deposition occurred mainly underwater, and the majority of macroscopic fossils, insect pores and root-lap structures developed during this stage. The stacking pattern is stacked imbricated regression, and the deposition center is at the delta front and the west side (Fig. 14, stage II). Isolated zonal deposition and fine-grained deposition are the main depositional patterns, the structure and composition maturity are medium, and the sand beds are thin or nonexistent. This stage is the transition from a single provenance to multiple provenances, and the vegetation was more developed. The third stage is a forced lacustrine regression system with aggradation to progradation and degradation stacking (APD) (Neal and Abreu, 2009) (Fig. 13(c)). The deposits are mainly fine sand, silt, and mudstone, with occasional lenticular gravelly channels, and the stacking pattern is a terrace-stepping progression with the center of deposition far from the delta front (Fig. 14, Stage III). Isolated zonal development and medium coarse-fine grain deposition were dominant. The high textural and compositional maturity, thin fine-grained sand beds, multi-provenance sediment supply, abundant vegetation, and surface terrace development indicate that the shoreline was rapidly receding toward the lake basin.

5.2 Controlling factors

5.2.1 Tectonics

There have been nine major tectonic deformation events (at 21. 8−7.78 Ma, 5.1 Ma, 3.7−3.4 Ma, 2.8−2.24 Ma, 1.91−1.75 Ma, 1.3−1.1 Ma, 0.9−0.7 Ma, and 0.15−0.12 Ma) on the north-eastern margin of the Qinghai-Xizang Plateau. The period 8−7.78 Ma represents the beginning of the strong tectonic deformation of the north-eastern Qinghai-Xizang Plateau, the period 3.7−3.4 Ma

Fig. 11 Partial enlarged detail of profile 7. (a) and (b) are gravelly sandstone deposits; (c) is debris flow to a traction flow; (d) and (e) are bioclastics; (f) is reed-related tufa; (g)and (i) are fossils; (j) and (k) are burrows with backfilling structures; (l) is root-lap structures.

represents the core of the tectonic deformation of the north-eastern Qinghai-Xizang Plateau, the period 1.91−1.75 Ma represents the strongest tectonic deformation and the folding and uplift of north-eastern edge of the Qinghai-Xizang Plateau, and the period 0.9−0.7 Ma represents the Kunlun-Yellow River movement on the north-eastern edge of the Tibetan Plateau. The present-day landforms were formed by the uplift associated with the Kunlun-Yellow River movement during 0.9−0.7 Ma (Yuan, 2003; An et al., 2006; Zhang et al., 2006; Yuan et al., 2013).

Due to the strong activity of the Nanshan boundary fault in Qinghai, the palaeotopography in the southern Qinghai Lake Basin has a steep slope, which played a great role in controlling the deposition of the delta (Lu, 2004; Wang and Burchfiel, 2004). The continuous activity of the Zongwulongshan-Nanshan fault in Qinghai has caused the Nanshan Mountains to continuously uplift and the lacustrine deposits to sink, forming multilevel terraces (Figs. 1 and 12) between the basin and the Nanshan range and causing the lacustrine deposits to recede rapidly, which is also the main factor controlling the mud-rich deposits in the Heimahe delta (Yuan et al., 1990). Additionally, the uplift of the Nanshan Mountain thrust continues to occur, resulting in a large topographic elevation difference between the hanging and foot walls of the fault, and the debris eroded from the upthrown side of the fault is directly deposited at the bottom of the foot wall, providing a large amount of readily available sediment for the Heimahe delta (Liu, 2002; Lu, 2004; Madsen et al., 2008).

The fault system controlling the deposition of the fan (Gawthorpe and Calella, 1990) has the following characteristics: (i) it is a boundary fault between the South Qilian tectonic zone and the Zongulong tectonic zone to the west of the Heimahe River and becomes a hidden fault in the study area because it is covered by the Quaternary system on the southern shore of Qinghai Lake; (ii) it has the characteristics of multistage activity and has controlled the distribution of the delta; (iii) it controls the distribution of the regional stratigraphy; and (iv) it is geomorphologically manifested as multistage terraces (Fig. 12). The contemporaneous activity of the fault increased the accommodation in the PA stage.

5.2.2 Climate change

The Heimahe area is a zone of relatively high precipitation due to the local topography, with a multiyear

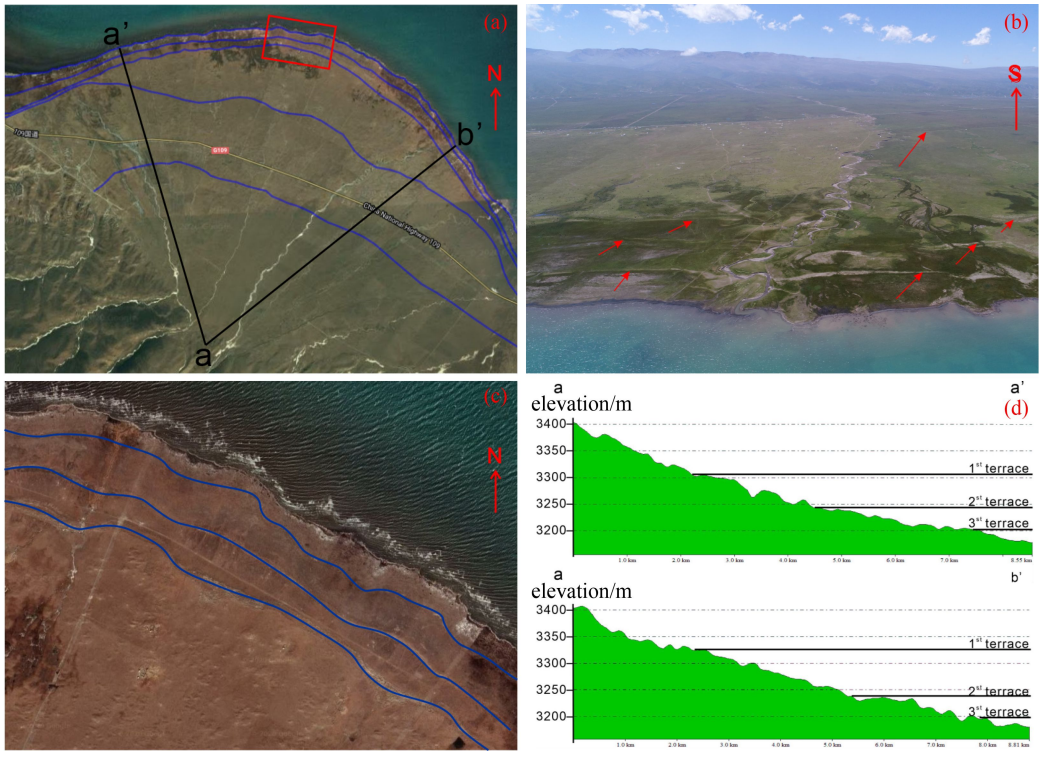

Fig. 12 Terraced trajectory. (a) Macroscopic characteristics of terraces in satellite image; (b) Panoramic photo of terrace; (c) enlarged red box in (a); (d) two lines elevation map in (a).

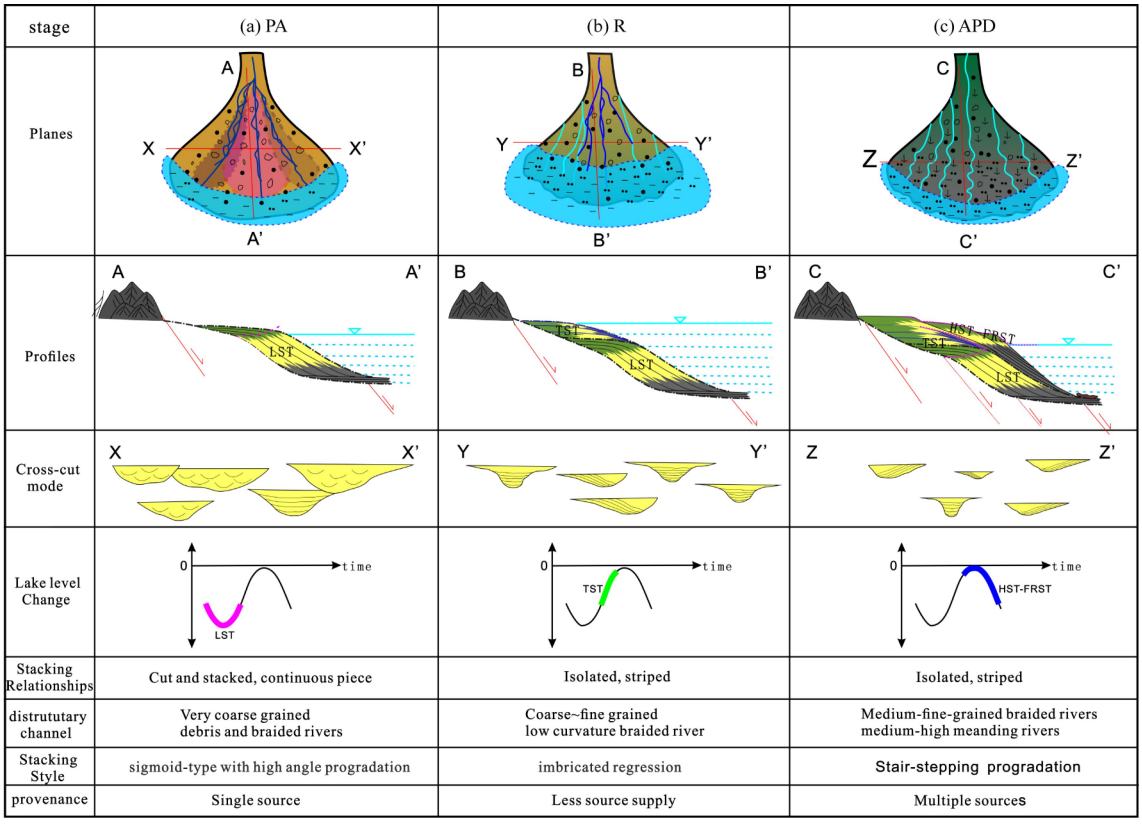

Fig. 13 Comparative table of three depositional stage characteristics. (a) characteristics of stage PA; (b) characteristics of stage R; (c) characteristics of stage APD.

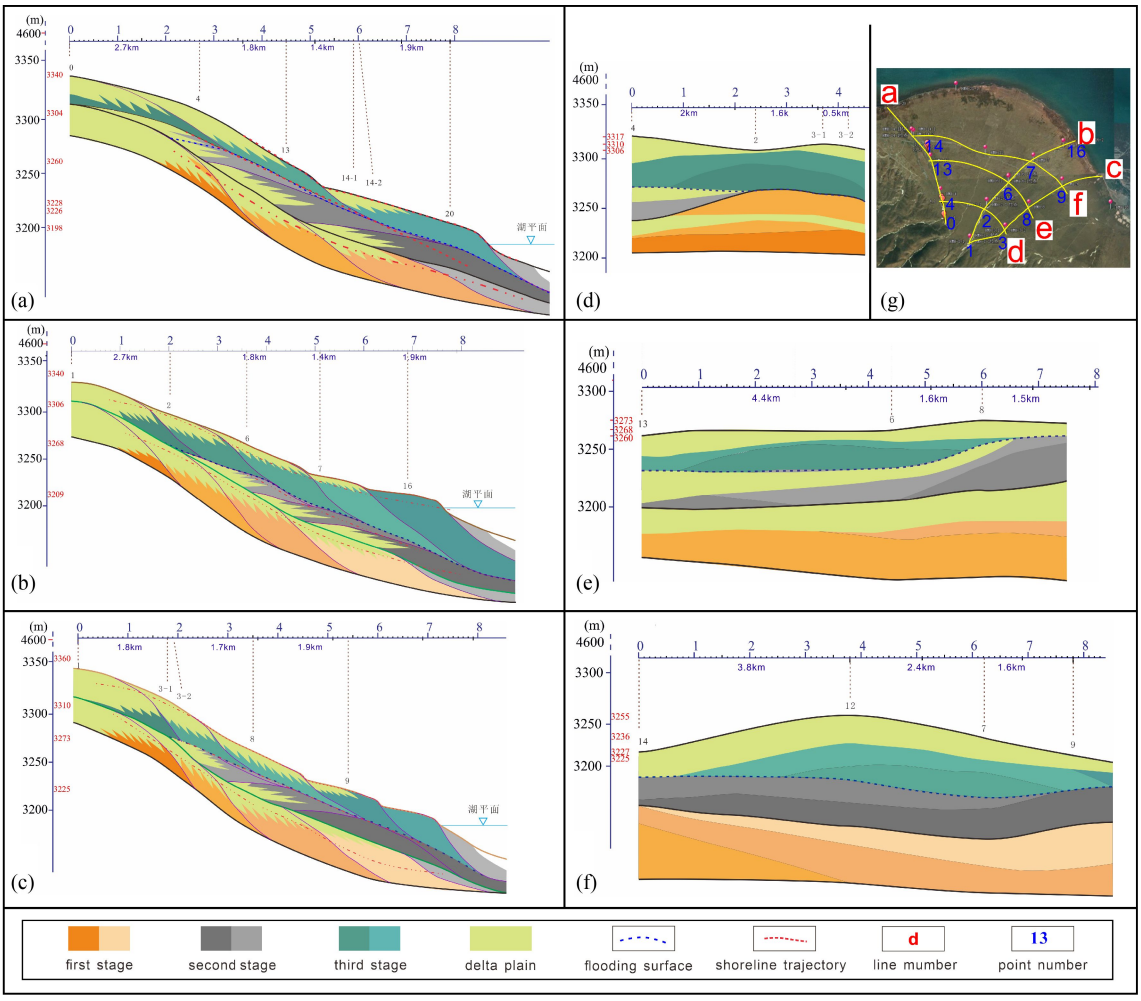

Fig. 14 Sedimentation pattern characteristics. (a)−(c) down-stream outcrop profiles; (d)−(f) cross-stream outcrop profiles; (g) location of (a)−(f).

average annual precipitation of 426 mm, but the precipitation is still much less than the evaporation (Holmes et al., 2009; Liu et al., 2010; Li et al., 2013; Wang and Feng, 2013; Li et al., 2017). The uplift of the Qinghai-Xizang Plateau and other tectonic movements are the main factors driving climate change in this region. Climate fluctuation is one of the factors affecting the change in the lake level. The climate of the study area has undergone three major changes between warm-humid and warm-dry conditions over approximately 10 kyrs (Shen et al., 2005; Liu et al., 2010; Lu et al., 2011; Lu et al., 2015; Hou et al., 2016; Tang et al., 2018; Zhang et al., 2020; Xue and Zeng, 2021) (Fig. 15). Stage A corresponds to the PA stage, and weathering and denudation were strong under relatively dry climate conditions; coarse-grained delta deposits formed in response to the sufficient sediment supply. Stage B corresponds to the R stage, and stage C corresponds to the APD stage. From the middle of stage B, the climate was relatively humid, and the grain size of the sediments became significantly finer. In late stage C, the lake level declined rapidly, corresponding to the forced lacustrine retreat stage.

5.2.3 Lake level variations

The lake experienced several periods of transgression and regression within 10 kyrs. Fault activity is frequent in the Heimahe area, and climate fluctuations are closely related to tectonic activity (Gawthorpe and Calella, 1990; Reading and Richards, 1994; Li et al., 2001). The lake level reached a maximum of approximately 3210 m at approximately 3 kyrs (Fig. 16) (Henderson and Holmes, 2009; Liu et al., 2011; Pan et al., 2012; Liu et al., 2013; Fan et al., 2014; Cui et al., 2016; Wang et al., 2019b; Xu et al., 2020). Tectonic movement and rainfall are important factors affecting changes in lake levels. The lake level increased significantly at 7.8 ka and 3.4 ka, while the precipitation did not increase significantly at 3.4 ka. Therefore, it is believed that the tectonic activity at this time caused the lake level to rise.

Lake level is one of the important factors affecting the distribution and stacking pattern of sedimentary bodies. The lacustrine development in the study area is mainly divided into three stages (Fig. 16). When the lake level was at a lower level and rose slowly in stage A (Figs.

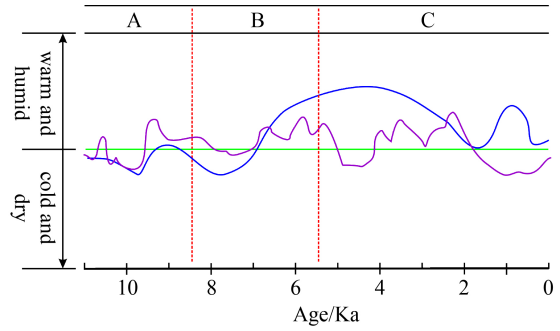

Fig. 15 Climate fluctuate in Qinghai Lake area in recent 10 kyrs.

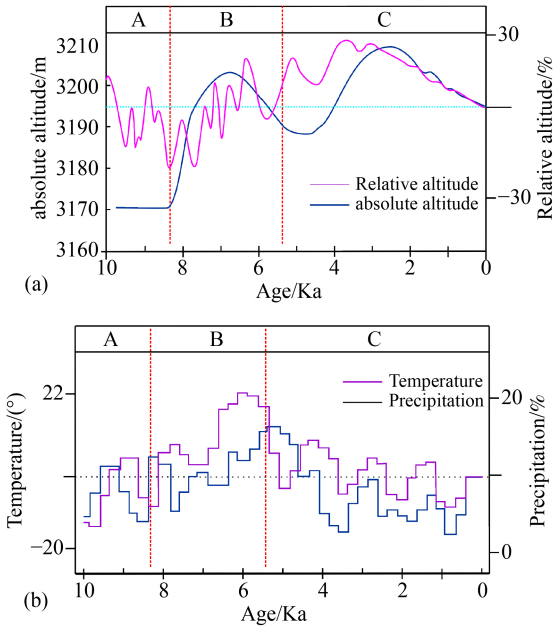

Fig. 16 Recent 10 kyrs Qinghai lake level changes. (a) Altitude; (b) temperature and precipitation.

16(a) and 16(b)), corresponding to stage I (Figs. 13(a) and 14), the delta body gradually retreated and had a fining-up trend. In stage B (Figs. 16(a) and 16(b)), corresponding to stage II (Figs. 13(b) and 14), the lake rose rapidly. The grain size of the sediments rapidly changed from coarse to fine. In stage C (Figs. 16(a) and 16(b)), corresponding to stage III (Figs. 13(c) and 14), the lake level rose to the maximum and then rapidly declined. After the deposit surface was exposed, some of the deposit was eroded, the delta gradually accumulated, the grain size became coarser, and the sedimentary range expanded.

6 Conclusions

1) The classification of delta architecture is determined by facies association. The delta plain can be divided into 4 types of architectural elements and their associations, namely, debris-flow channels, switched channels, migrated channels, and vertical accretion bars, and the delta front can be divided into 4 types of architectural elements and their associations, namely, filled channels, bilateral accretion bars, migrated channels, and unilateral bars.

2) The sedimentary evolution process is divided into three stages: PA, R, and APD. In the PA stage, the stacking pattern is an inverse S-type high-angle progression, dominated by coarse-grained sedimentation, which was caused by an abundant sediment supply, and the deposits formed in superimposed channels and continuous sheets. In the R stage, the stacking pattern is imbricated, dominated by fine-grained sedimentation, and the channels are isolated and stripe-shaped. The stacking pattern of the APD is a stair-stepping progression, characterized by fine-grained sediments deposited in isolated strips.

3) Tectonic activity, climate fluctuations and lake level variations jointly controlled the planar distribution, superimposed pattern of sand bodies and evolution of the delta, and tectonics were the most important controlling factor. The climate and the palaeostructure characteristics controlled the sediment supply.

Since the sediments of the studied section are not yet dated and cannot be positively related to the changes in the lake level, the sedimentary evolution of the study area needs to be further studied.

Acknowledgments This study was co-funded by the Natural Science Foundation of China (Grant Nos. 42172112 and 42272124), Fundamental Research Funds for the Central Universities (No. 2-9-2019-100), and Major State Science and Technology Research Program (Nos. 2016ZX05024-002 and 2017ZX05001-002).

Competing interests The authors declare that they have no competing interests.

References

Afuso H, Matsubara H (2019). Development of rock outcrops inspection system using UAV and VR technology. ISRM Young Scholars Symposium on Rock Mechanics

Allen J R L (1983). Studies in fluviatile sedimentation: bars, bar-complexes and sandstone sheets (low-sinuosity braided streams) in the Brownstones (L. Devonian), Welsh Borders. Sediment Geol, 33: 237–293

An Z S, Zhang P Z, Wang E Q, Wang S M, Qiang X K, Li L, Song Y G, Chang H, Liu X D, Zhou W J, Liu W G, Cao J Y, Li X Q, Shen J, Liu Y, Ai L (2006). Changes of the monsoom-arid environment in China and growth of the Tibetan Plateau since the Miocece. Quatern Res, (5): 678–693

Backert N, Ford M, Malartre F (2010). Architecture and sedimentology of the kerinitis Gilbert-type fan delta, Corinth Rift, Greece. Sedimentology, 57(2): 543–586

Bemis S P, Micklethwaite S, Turner D, James M R, Akciz S, Thiele S T, Bangash H A (2014). Ground-based and UAV-based

photogrammetry: a multi-scale, high-resolution mapping tool for structural geology and paleoseismology. J Struct Geol, 69: 163–178

Bian Q T, Liu J L, Luo X P and Xiao J L (2000). Geotectonic setting, formation and evolution of the Qinghai Lake. Seismic Geol, 22(1): 20–26

Blistan P, Kovanic L, Zeliznakova V, Palkova J (2016). Using UAV photogrammetry to document rock outcrops. Acta Montan Slovaca, 21(2): 154–161

Bridge J S, Jalfin G A, Georgieff S M (2000). Geometry, lithofacies, and spatial distribution of cretaceous fluvial sandstone bodies, San Jorge Basin, Argentina: outcrop analog for the hydrocarbon-bearing Chubut Group. J Sediment Res, 70(2): 341–359

Burnham B S, Hodgetts D (2019). Quantifying spatial and architectural relationships from fluvial outcrops. Geosphere, 15(1): 236–253

Butler R W H, Mccaffrey W D (2010). Structural evolution and sediment entrainment in mass-transport complexes: outcrop studies from Italy. J Geol Soc London, 167(3): 617–631

Chang H, An Z S, Wu F (2008). Major element records from the Qinghai Lake Basin—Gonghe Basin sediments indicating the Nanshan (Qinghai) uplift event. Quatern Res, (5): 36–44

Chang H, Jin Z, An Z (2009). Sedimentary evidences of the uplift of the Qinghai Nanshan (the mountains south to Qinghai Lake) and its implication for structural evolution of the Lake Qinghai—Gonghe Basin. Geological Review(1): 49–57

Chen J (2016). The Study on Mordern Sedimentary System in the Qinghai Lake. Dissertation for Doctoral Degree. Beijing: China University of Geosciences

Chen J, Jiang Z X, Zhang W Y, Liu C, Han C (2020). The study on the modern sedimentary system of Buha River Delta in Qinghai Lake. Geol J, 55(7): 5216–5232

Chen J, Jiang Z, Zhang W, Liu C, Xu W (2018). The development model of modern eolian facies dominated by "source-sink" depositional system: a case study of the east coast of Qinghai Lake. China Desert, 38(5): 999–1008

Cui B L, Li X Y, Wei X H (2016). Isotope and hydrochemistry reveal evolutionary processes of lake water in Qinghai Lake. J Great Lakes Res, 42(3): 580–587

Deynoux M, Çiner A, Monod O, Karabıyıkoglu M, Manatschal G, Tuzcu S (2005). Facies architecture and depositional evolution of alluvial fan to fan-delta complexes in the tectonically active Miocene Köprüçay Basin, Isparta Angle, Turkey. Sediment Geol, 173(1–4): 315–343

Ding Z Y, Lu R J, Lyu Z Q, Liu X K (2019). Geochemical characteristics of Holocene aeolian deposits east of Qinghai Lake, China, and their paleoclimatic implications. Sci Total Environ, 692: 917–929

Eilertsen R S, Corner G D, Aasheim O, Hansen L (2011). Facies characteristics and architecture related to palaeodepth of Holocene Fjord-delta sediments. Sedimentology, 58(7): 1784–1809

Enge H D, Buckley S J, Rotevatn A, Howell J A (2007). From outcrop to reservoir simulation model: workflow and procedures. Geosphere, 3(6): 469–490

Fabuel-Perez I, Hodgetts D, Redfern J (2009). A new approach for outcrop characterization and geostatistical analysis of a low-sinuosity fluvial-dominated succession using digital outcrop models: Upper Triassic Oukaimeden Sandstone Formation, central High Atlas, Morocco. AAPG Bull, 93(6): 795–827

Fan Q S, Ma H Z, Wei H C, An F Y (2014). Holocene lake-level changes of Hurleg Lake on Northeastern Qinghai-Tibetan Plateau and possible forcing mechanism. Holocene, 24(3): 274–283

Fielding C R, Alexander J, Allen J P (2018). The role of discharge variability in the formation and preservation of alluvial sediment bodies. Sediment Geol, 365: 1–20

Freitas B T, Silva L H G, Almeida R P, Galeazzi C P, Figueiredo H G, Tamura L N, Janikian L, Figueiredo F T, Assine M L (2021). Cross-strata palaeocurrent analysis using virtual outcrops. Sedimentology, 68(6): 2397–2421

Fu C, Li S L, Li S L, Fan X, Xu J Y (2020). Sedimentary characteristics, dispersal patterns, and pathway formation in Liaoxi Sag, Liaodong Bay Depression, north China: evolution of source-to-sink systems in strike-slip tectonics belt. Geol J, 55(7): 5119–5137

García-García F, Corbi H, Soria J M, Viseras C (2011). Architecture analysis of a river flood-dominated delta during an overall sea-level rise (early Pliocene, SE Spain). Sediment Geol, 237(1–2): 102–113

García-García F, Fernández J, Viseras C, Soria J M (2006). Architecture and sedimentary facies evolution in a delta stack controlled by fault growth (Betic Cordillera, southern Spain, Late Tortonian). Sediment Geol, 185(1–2): 79–92

Gawthorpe R L, Calella A (1990). Tectonic controls on coarse-grained delta depositional systems in rift basins. Sediment, 10: 113–127

Ghazi S, Mountney N P (2009). Facies and architectural element analysis of a meandering fluvial succession: the Permian Warchha Sandstone, Salt Range, Pakistan. Sediment Geol, 221(1–4): 99–126

Henderson A C G, Holmes J A (2009). Palaeolimnological evidence for environmental change over the past millennium from Lake Qinghai sediments: a review and future research prospective. Quat Int, 194(1–2): 134–147

Hodgetts D (2013). Laser scanning and digital outcrop geology in the petroleum industry: a review. Mar Pet Geol, 46: 335–354

Holmes J A, Cook E R, Yang B (2009). Climate change over the past 2000 years in western China. Quat Int, 194(1–2): 91–107

Homewood P, Razin P, Grélaud C, Droste H, Vahrenkamp V, Mettraux M, Mattner J (2008). Outcrop sedimentology of the Natih Formation, northern Oman: a field guide to selected outcrops in the Adam Foothills and Al Jabal al Akhdar areas. Geo-Arabia, 13(3): 39–120

Horton B K, Schmitt J G (1996). Sedimentology of a lacustrine fan-delta system, Miocene horse camp formation, Nevada, USA. Sedimentology, 43(1): 133–155

Hou J Z, Huang Y S, Zhao J T, Liu Z H, Colman S, An Z S (2016). Large Holocene summer temperature oscillations and impact on the peopling of the Northeastern Tibetan plateau. Geophys Res Lett, 43(3): 1323–1330

Janocha J, Smyrak-Sikora A, Senger K, Birchall T (2021). Seeing beyond the outcrop: integration of ground-penetrating radar with digital outcrop models of a paleokarst system. Mar Pet Geol, 125: 104833

Lanzhou Institute of Geology CAS (1979). Comprehensive Survey Report of Qinghai Lake. Beijing: Science Press

Li B Y, Wang S M, Zhu L P, Li Y F (2001). 12 ka BP lake environment on the Tibetan Plateau. Sci China Ser D Earth Sci, 44(S1): 324–331

Li J Y, Dodson J, Yan H, Cheng B, Zhang X, Xu Q, Ni J, Lu F (2017). Quantitative precipitation estimates for the northeastern Qinghai-Tibetan plateau over the last 18000 years. J Geophys Res Atmos, 122(10): 5132–5143

Li S L, Ma Y Z, Yu X, Jiang P, Li M, Li M (2014). Change of deltaic depositional environment and its impacts on reservoir properties—a braided delta in South China Sea. Mar Pet Geol, 58: 760–775

Li S L, Yu X H, Chen B T, Li S L (2015a). Quantitative characterization of architecture elements and their response to base-level change in a sandy braided fluvial system at a mountain front. J Sediment Res, 85(10): 1258–1274

Li S L, Yu X H, Chen B T, Li S L (2015b). Quantitative characterization of architecture elements and their response to base-level change in a sandy braided fluvial system at a mountain front. J Sediment Res, 85(10): 1258–1274

Li S L, Yu X H, Steel R, Zhu X M, Li S L, Cao B, Hou G W (2018). Change from tide-influenced deltas in a regression-dominated set of sequences to tide-dominated estuaries in a transgression-dominated sequence set, East China Sea Shelf Basin. Sedimentology, 65(7): 2312–2338

Li Y, Wang N, Li Z, Ma N, Zhou X, Zhang C (2013). Lake evaporation: a possible factor affecting lake level changes tested by modern observational data in arid and semi-arid China. J Geogr Sci, 23(1): 123–135

Liu B B, Tan C P, Yu X H, Qu J H, Zhao X M, Zhang L (2019a). Sedimentary characteristics and controls of a retreating, coarse-grained fan-delta system in the lower Triassic, Mahu Depression, northwestern China. Geol J, 54(3): 1141–1159

Liu F G, Zhang Y, Feng Z, Hou G, Zhou Q, Zhang H (2010). The impacts of climate change on the neolithic cultures of Gansu-Qinghai region during the Late Holocene megathermal. J Geogr Sci, 20(3): 417–430

Liu X (2002). A 16000-year pollen record of Qinghai Lake and its paleoclimate and paleoenvironment. Chin Sci Bull, 47(22): 1931–1936

Liu X J, Cong L, An F Y, Miao X D, E C Y (2019b). Downwind aeolian sediment accumulations associated with lake-level variations of the Qinghai lake during the Holocene, northeastern Qinghai-Tibetan Plateau. Environ Earth Sci, 78(1): 19

Liu X J, Lai Z P, Madsen D, Yu L P, Liu K, Zhang J R (2011). Lake level variations of Qinghai lake in northeastern Qinghai-Tibetan Plateau since 3.7 ka based on OSL dating. Quat Int, 236(1–2): 57–64

Liu X J, Lai Z P, Zeng F M, Madsen D B, E C Y (2013). Holocene lake level variations on the Qinghai-Tibetan Plateau. Int J Earth Sci, 102(7): 2007–2016

Liu X X, Vandenberghe J, An Z S, Li Y, Jin Z D, Dong J B, Sun Y B (2016). Grain size of lake Qinghai sediments: implications for riverine input and Holocene monsoon variability. Palaeogeogr Palaeoclimatol Palaeoecol, 449: 41–51

Lu H Y (2004). Geomorphologic evidence of phased uplift of the northeastern Qinghai-Tibet Plateau since 14 million years ago. Sci China Ser D Earth Sci, 47(9): 822–833

Lu H Y, Zhao C F, Mason J, Yi S W, Zhao H, Zhou Y L, Ji J F, Swinehart J, Wang C M (2011). Holocene climatic changes revealed by aeolian deposits from the Qinghai Lake area (northeastern Qinghai-Tibetan Plateau) and possible forcing mechanisms. Holocene, 21(2): 297–304

Lu R J, Jia F F, Gao S Y, Shang Y, Li J F, Zhao C (2015). Holocene aeolian activity and climatic change in Qinghai Lake Basin, northeastern Qinghai-Tibetan Plateau. Palaeogeogr Palaeoclimatol Palaeoecol, 430: 1–10

Maddy D (2002). An evaluation of climate, crustal movement and base level controls on the Middle-Late Pleistocene development of the River Severn, UK. Neth J Geosci, 81(3–4): 329–338

Madsen D B, Haizhou M, Rhode D, Brantingham P J, Forman S L (2008). Age constraints on the late Quaternary evolution of Qinghai Lake, Tibetan Plateau. Quat Res, 69(2): 316–325

Marques A Jr, Horota R K, de Souza E M, Kupssinskü L, Rossa P, Aires A S, Bachi L, Veronez M R, Gonzaga L Jr, Cazarin C L (2020). Virtual and digital outcrops in the petroleum industry: a systematic review. Earth Sci Rev, 208: 103260

Meng W C, Chen Y B, Chen L J, Li J X (2020). Study of sedimentary succession and its origin of gravel beach bar: a case from the modern beach bar in the southeastern Qinghai Lake. Northwestern Geol, 53(3): 56–65

Miall A D (1985). Architectural-element analysis - A new method of facies analysis applied to fluvial deposits. Earth Sci Rev, 22(4): 261–308

Miall A D (2002). Architecture and sequence stratigraphy of Pleistocene fluvial systems in the Malay Basin, based on seismic time-slice analysis. AAPG Bull, 86(7): 1201–1216

Miall A D, Jones B G (2003). Fluvial architecture of the Hawkesbury Sandstone (Triassic), near Sydney, Australia. J Sediment Res, 73(4): 531–545

Morgan A M, Craddock R A (2017). Depositional processes of alluvial fans along the Hilina Pali fault scarp, Island of Hawaii. Geomorphology, 296: 104–112

Moscariello A (2018). Alluvial fans and fluvial fans at the margins of continental sedimentary basins: geomorphic and sedimentological distinction for geo-energy exploration and development. Spec Publ Geol Soc Lond, 440(1): 215–243

Nagendra R, Raja R, Reddy A N, Jaiprakash B C, Bhavani R (2002). Outcrop sequence stratigraphy of the Maastrichtian Kallankurchchi Formation, Ariyalur group, Tamil Nadu. J Geol Soc India, 59(3): 243–248

Neal and Abreu (2009). Sequence stratigraphy hierarchy and the accommodation succession method. Geology, 37(9): 778–782

Nocita B W, Lowe D R (1990). Fan-delta sequence in the Archean Fig Tree Group, Barberton Greenstone-Belt, South-Africa. Precambrian Res, 48(4): 375–393

Olariu C, Bhattacharya J P (2006). Terminal distributary channels and delta front architecture of river-dominated delta systems. J Sediment Res, 76(1–2): 212–233

Pan B L, Yi C, Jiang T, Dong G, Hu G, Jin Y (2012). Holocene lake-level changes of Linggo Co in central Tibet. Quat Geochronol, 10: 117–122

Paterson G A, Heslop D (2015). New methods for unmixing sediment grain size data. Geochem Geophys Geosyst, 16(12): 4494–4506

Pickel A, Frechette J D, Comunian A, Weissmann G S (2015). Building a training image with digital outcrop models. J Hydrol (Amst), 531: 53–61

Plink-Björklund P, Steel R J (2004). Initiation of turbidity currents: outcrop evidence for Eocene hyperpycnal flow turbidites. Sediment Geol, 165(1–2): 29–52

Qiang M R, Chen F H, Song L, Liu X X, Li M Z, Wang Q (2013). Late Quaternary aeolian activity in Gonghe Basin, northeastern Qinghai-Tibetan Plateau, China. Quat Res, 79(3): 403–412

Qinghai Bureau of Geology and Mineral Resources Q (1991). Regional Geology of Qinghai Province. Beijing: Geological Publishing House

Reading H G, Richards M (1994). Turbidite systems in deep-water basin margins classified by grain-size and feeder system. AAPG Bull, 78(5): 792–822

Rioult M, Dugue O, Duchene R J, Ponsot C, Fily G, Moron J M, Vail P R (1991). Outcrop sequence stratigraphy of the Anglo-Paris Basin, Middle to Upper Jurassic (Normandy, Maine, Dorset). Bull Cent Rech Explor Prod Elf-Aquitaine, 15(1): 101–194

Rohais S, Eschard R, Guillocheau F (2008). Depositional model and stratigraphic architecture of rift climax Gilbert-type fan deltas (Gulf of Corinth, Greece). Sediment Geol, 210(3–4): 132–145

Shan X, Li S L, Li S L, Yu X H, Wan L, Jin L N, Wang T Y (2018). Sedimentology of a topset-dominated, braided river delta of Huangqihai Lake, north China: implications for formation mechanisms. J Paleolimnol, 59(2): 245–261

Shan X, Shi X F, Clift P D, Seddique A A, Liu S F, Tan C P, Liu J G, Hasan R, Li J C, Song Z J (2021). Sedimentology of the modern seasonal lower Ganges river with low inter-annual peak discharge variance, Bangladesh. J Geol Soc London, 178(1): jgs2020–094

Sharifigaliuk H, Mahmood S M, Ahmad M, Rezaee R (2021). Use of outcrop as substitute for subsurface shale: current understanding of similarities, discrepancies, and associated challenges. Energy Fuels, 35(11): 9151–9164

Shen J, Liu X Q, Wang S M, Matsumoto R (2005). Palaeoclimatic changes in the Qinghai Lake area during the last 18000 years. Quat Int, 136(1): 131–140

Song C H, Fang X M, Shi Y M, Wang X M (2000). Characteristics and genesis of eolian dunes on the west bank of Qinghai Lake. China Desert, 20(4): 443–446

Song C H, Fang X M, Shi Y M, Wang X M (2001). Sedimentary characteristics of modern lacustrine deltas in Qinghai Lake and their controlling factors. J Lanzhou U (Nat Sci), 37(3): 112–121

Tan C P, Yu X H, Li S L, Shan X, Chen B T (2016). Sedimentology and stratigraphic evolution of the fan delta at the Badaowan Formation (Lower Jurassic), Southern Junggar Basin, Northwest China. Arab J Geosci, 9(2): 115

Tan C P, Yu X H, Liu B B, Qu J H, Zhang L, Huang D J (2017). Conglomerate categories in coarse-grained deltas and their controls on hydrocarbon reservoir distribution: a case study of the Triassic Baikouquan Formation, Mahu Depression, NW China. Petrol Geosci, 23(4): 403–414

Tanaka J, Maejima W (1995). Fan-delta sedimentation on the basin margin slope of the cretaceous, strike-slip Izumi Basin, Southwestern Japan. Sediment Geol, 98(1–4): 205–213

Tang L Y, Duan X F, Kong F J, Zhang F, Zheng Y F, Li Z, Mei Y, Zhao Y W, Hu S J (2018). Influences of climate change on area variation of Qinghai Lake on Qinghai-Tibetan Plateau since 1980s. Sci Rep, 8(1): 7331

Trendell A M, Atchley S C, Nordt L C (2013). Facies analysis of a probable large-fluvial-fan depositional system: the Upper Triassic Chinle formation at petrified forest national park, Arizona, U. S. A. J Sediment Res, 83(10): 873–895

Tunbridge I P (1981). Sandy high-energy flood sedimentation—Some criteria for recognition, with an example from the Devonian of SW England. Sediment Geol, 28(2): 79–95

Ulicny D (2001). Depositional systems and sequence stratigraphy of coarse-grained deltas in a shallow-marine, strike-slip setting: the Bohemian Cretaceous Basin, Czech Republic. Sedimentology, 48(3): 599–628

Wakefield O J W, Hough E, Peatfield A W (2015). Architectural analysis of a Triassic fluvial system: the Sherwood Sandstone of the East Midlands Shelf, UK. Sediment Geol, 327: 1–13

Wang E C, Burchfiel B C (2004). Late Cenozoic right-lateral movement along the Wenquan fault and associated deformation: implications for the kinematic history of the Qaidam Basin northeastern Tibetan Plateau. Int Geol Rev, 46(10): 861–879

Wang J, Li X B, Liu H Q (2019a). Study of the development and preservation of lacustrine beach and bar based on the modern sedimentary characteristics of Qinghai lake. J Sediment, 37(5): 1016–1030

Wang Q, Sha Z, Wang J, Du J, Hu J, Ma Y (2019b). Historical changes in the major and trace elements in the sedimentary records of Lake Qinghai, Qinghai-Tibet Plateau: implications for anthropogenic activities. Environ Geochem Health, 41(5): 2093–2111

Wang W, Feng Z D (2013). Holocene moisture evolution across the Mongolian plateau and its surrounding areas: a synthesis of climatic records. Earth Sci Rev, 122: 38–57

White C D, Willis B J (2000). A method to estimate length distributions from outcrop data. Math Geol, 32(4): 389–419

Winsemann J, Asprion U, Meyer T, Schramm C (2007). Facies characteristics of Middle Pleistocene (Saalian) ice-margin subaqueous fan and delta deposits, glacial Lake Leine, NW Germany. Sediment Geol, 193(1–4): 105–129

Wu Y, Zhang T, Zhang Z, Cui H (2010). Types and characteristics of depositional systems tract and its petroleum geological significance. Journal of Palaeogeography, 12(1): 69–81

Xu X F, Yuan L G, Jiang Z S, Chen C F, Cheng S (2020). Lake level changes determined by cryosat-2 altimetry data and water-induced loading deformation around lake Qinghai. Adv Space Res, 66(11): 2568–2582

Xue H P, Zeng F M (2021). Holocene environmental evolution in the Qinghai Lake area recorded by aeolian deposits. Quat Int, 580: 67–77

Yin Z J, Zhang B, Hu Y, Zhu J, Guo C, Chen G, Hou X, Liu J, Zhang R (2020). The facies analysis of a fan delta by integrating multiple discipline data - A case study of the KL-A Oilfield, Bohai Bay Basin, China. Interpretation, 8(2): SF21–SF35

Young R A, Slatt R M, Staggs J G (2003). Application of ground penetrating radar imaging to deepwater (turbidite) outcrops. Mar Pet Geol, 20(6–8): 809–821

Yu X H, Li S L, Tan C P, Huo J H, Zhang C, Zhao C F (2018b). Coarse coarse-grained deposits and the irreservoir characterizations: a look back to see forward and hot issues. J Palaeogeogr, 20(5): 713–726

Yu X H, Li S L, Tan C P, Xie J, Chen B T, Yang F (2013). The response of deltaic systems to climatic and hydrological changes in Daihai Lake rift basin, Inner Mongolia, northern China. J Palaeogeogr, 2(1): 41–55

Yu X, Li S, Li S (2018a). Clastic Hydrocarbon Reservoir Sedimentology. NewYork: Springer

Yuan B, Chen K, Bowler J M, Ye S (1990). The formation and evolution of the Qinghai lake. Quaterern Sci, 3: 233–243

Yuan D (2003). Tectonic deformation features and space-time evolution in Northeastern margin of the Qinghai-Tibetan Plateau since the Late Cenozoic time. Dissertation for Doctor Degree. Beijing: Institute of Geology, China Earthquake Administration

Yuan D Y, Ge W P, Chen Z W, Li C Y, Wang Z C, Zhang H P, Zhang P Z, Zheng D W, Zheng W J, Craddock W H, Dayem K E, Duvall A R, Hough B G, Lease R O, Champagnac J D, Burbank D W, Clark M K, Farley K A, Garzione C N, Kirby E, Molnar P, Roe G H (2013). The growth of northeastern Tibet and its relevance to large-scale continental geodynamics: a review of recent studies. Tectonics, 32(5): 1358–1370

Zhang C M, Zhu R, Yin T J and Yin Y S (2015). Advances in fan deltaic sedimentology. Xinjiang Petrol Geol, 36(3): 110–116

Zhang G Q, Yao T D, Xie H J, Yang K, Zhu L P, Shum C K, Bolch T, Yi S, Allen S, Jiang L G, Chen W F, Ke C Q (2020). Response of Tibetan plateau lakes to climate change: trends, patterns, and mechanisms. Earth Sci Rev, 208: 103269

Zhang H F, Chen Y L, Xu W C, Liu R, Yuan H L, Liu X M (2006). Granitoids around Gonghe Basin in Qinghai province: petrogenesis and tectonic implications. Acta Petrol Sin, 22(12): 2910–2922

Zhang X N, Zhou A, Wang X, Song M, Zhao Y, Xie H, Russell J M, Chen F (2018a). Unmixing grain-size distributions in lake sediments: a new method of endmember modeling using hierarchical clustering. Quat Res, 89(1): 365–373

Zhang Y F, Hu C L, Wang M, Ma M F, Wang X M, Jiang Z X (2018b). A quantitative sedimentary model for the modern lacustrine beach bar (Qinghai Lake, northwest China). J Paleolimnol, 59(2): 279–296

Zhao J F, Mountney N P, Liu C Y, Qu H J, Lin J Y (2015). Outcrop architecture of a fluvio-lacustrine succession: Upper Triassic Yanchang Formation, Ordos Basin, China. Mar Pet Geol, 68: 394–413

Zielinski T, Gozdik J (2001). Palaeoenvironmental interpretation of a Pleistocene alluvial succession in central Poland: sedimentary facies analysis as a tool for palaeoclimatic inferences. Boreas, 30(3): 240–253